

**DESIGN A PORTABLE FIBER LASER SENSOR FOR RAILWAY
HEALTH ANALYSIS**

TAN CHAN LINN

**A project report submitted in partial fulfilment of the
requirements for the award of Bachelor of Science (Honours) Physics**

**Lee Kong Chian Faculty of Engineering and Science
Universiti Tunku Abdul Rahman**

May 2024

DECLARATION

I hereby declare that this project report is based on my original work except for citations and quotations which have been duly acknowledged. I also declare that it has not been previously and concurrently submitted for any other degree or award at UTAR or other institutions.

Signature : Chan Linn

Name : TAN CHAN LINN


ID No. : 2102050

Date : 15 September 2024

APPROVAL FOR SUBMISSION


I certify that this project report entitled “**DESIGN A PORTABLE FIBER LASER SENSOR FOR RAILWAY ANALYSIS**” was prepared by **TAN CHAN LINN** has met the required standard for submission in partial fulfilment of the requirements for the award of Bachelor of Science (Honours) Physics at Universiti Tunku Abdul Rahman.

Approved by,

Signature : 

Supervisor : Dr. Pua Chang Hong

Date : 18/9/2024

Signature : 

Co-Supervisor : Dr. Shee Yu Gang

Date : 18/9/2024

ABSTRACT

Railway systems are widely used globally for both passenger and freight transportation, with extensive network in countries like the USA, China and Russia. In Malaysia, there are 11 types of train systems, including freight and passenger railways, with a total length over 2700 km, mostly operated by Keretapi Tanah Melayu Berhad (KTMB). However, railway accidents and incidents have been a concern, with factors like collisions, derailments and mechanical failures contributing to these incidents. Apart from human error which can be reduced by automate railway and train control system. The reduction of derailment and failure of equipment can be achieved through the enhancement of sensors system or method used for detecting railway defects and the improvement of the railway health monitoring system.

Acoustic emission sensors and real-time transient modelling methods have been applied in many industries for quite some time. In railway monitoring, neighboring countries have already proposed new method that gives significant advantages compared to traditional methods. This project proposes an alternative method using a laser dynamics fiber sensor to monitor the vibration and acoustic waves of the train structure during operation.

Fiber laser sensor is known to have several good qualities such as immunity to electromagnetic interference, ability to cover long distances without signal degradation, light weight and safe to use. The performance of the sensor system is tested and it showed that the fiber sensor is effective when applied as railway health monitoring.

The copyright of this report belongs to the author under the terms of the copyright Act 1987 as qualified by Intellectual Property Policy of Universiti Tunku Abdul Rahman. Due acknowledgement shall always be made of the use of any material contained in, or derived from, this report.

© 2024, Tan Chan Linn. All right reserved.

TABLE OF CONTENTS

CHAPTER 1

1	INTRODUCTION	1
	1.1 Railway System in Malaysia	1
	1.2 Existing Sensors for Detecting Railway Defects and Tracks Irregularities	2
	1.3 Fiber Optic Sensors in Railway Monitoring	3
	1.4 Problem Statement	4
	1.5 Aims and Objectives	5
	1.6 Project Scope	5
	1.7 Outline of the Report	6

CHAPTER 2

2	LITERATURE REVIEW	7
	2.1 Theory	7
	2.1.1 Stimulated Emission and Population Inversion	7
	2.1.2 Laser Principle	8
	2.1.3 Fiber Optics	9
	2.1.4 Erbium Doped Fiber Laser (EDFL)	10
	2.2 Working Principle	11
	2.2.1 Laser Dynamics in EDFL	11
	2.2.2 Loss Modulation	15

CHAPTER 3

3	METHODOLOGY AND WORK PLAN	16
	3.1 Working Plan	16
	3.1.1 Stage 1: Study on the EDFL sensor	16
	3.1.2 Stage 2: Design and Build Prototype	22
	3.1.3 Stage 3: Installation and Pre-Testing on Test Bed	22
	3.1.4 Stage 4: Data Collection, Signal Processing and Noise Filtering	23
	3.1.5 Stage 5: Anomalies Detection	24

3.2	Prototype Design	24
3.2.1	Overall Prototype	24
3.2.2	Sensor Packaging	26
3.3	Optical Components	27
3.3.1	Laser Diode	27
3.3.2	Photodiode	28
3.4	Data Collection	28
3.4.1	Raspberry Pi Pico	29
CHAPTER 4		
4	RESULT AND DISCUSSIONS	31
4.1	Introduction	31
4.2	Fiber Laser Sensor	31
4.3	Characteristics of the sensors	32
4.3.1	Response of sensor in time domain	32
4.3.2	Response of Sensor in Frequency Domain	37
4.4	Data Acquisition	38
4.4.1	Signal Processing	38
4.5	Results	42
4.5.1	Normal Conditions	42
4.5.2	Weighted Condition	45
4.5.3	Obstacles conditions	46
4.6	Summary	47
CHAPTER 5		
5	CONCLUSION AND RECOMMENDATIONS	48
5.1	Conclusion	48
5.2	Improvements	48
5.3	Recommendations for Future Work	49
REFERENCES		50
APPENDICES		54

LIST OF TABLES

Table 1.1: Number of Passengers for Rail Transport Services, 2023	1
Table 2.1: Symbols from the Laser Dynamics and their Definition	11
Table 4.1: Table of Peak Amplitude of Sensors with Different Length	34

LIST OF FIGURES

Figure 1.1: Factors contributing to the rail accidents and incidents in Malaysia (Shahrir and Manan, 2021)	2
Figure 2.1: (a) Absorption, (b) Spontaneous emission, and (c) Stimulated emission (Kasap, 2013)	8
Figure 2.2: Simplified Energy levels of Er ³⁺ ions in Erbium-doped fiber (Zhu, Li, and Helmy, 2007)	9
Figure 2.3: Ring cavity of EDFL (Causado-Buelvas, Gomez-Cardona and Torres, 2011)	10
Figure 2.4: Simulation of Optical Power Fluctuation after an impact (Pua, Chong and Ahmad, 2013)	12
Figure 2.5: Illustration of optical microphone experiment setup (Pua et al., 2011)	13
Figure 2.6: Comparison of (a) background noise without acoustic signal (b) with 2 kHz of acoustic signal between electrical and optical microphones (Pua et al., 2011).	14
Figure 2.7: Loss modulation behavior of EDFL sensor (Woon et al., 2018)	14
Figure 3.1: Experimental setup of the EDFL acoustic sensor	16
Figure 3.2: Laser Source Module	17
Figure 3.3: WDM	17
Figure 3.4: Photodetector (THORLABS, DET08CFC/M)	17
Figure 3.5: PicoScope 3000 series	17
Figure 3.6: Optical Spectrum Analyzer (OSA)	18
Figure 3.7: OSA results at (A) backward port and (B) forward port	19
Figure 3.8: PicoScope 7 T&M	20
Figures 3.9: Splicing Tools	20
Figure 3.10: Fiber sensors made of SMF	21
Figure 3.11: Output Waveform in PicoScope when the sensor is tapped	21

Figure 3.12:	Track and Train simulation	23
Figure 3.13:	Laser Diode Driver	24
Figure 3.14:	Photodiode driver circuit (Thorlabs)	25
Figure 3.15:	Schematic Diagram of the Sensor Prototype	25
Figure 3.16:	AutoCAD Drawing	26
Figure 3.17:	Sensor Packaging	27
Figure 3.18:	Pigtailed Laser Diode	27
Figure 3.19:	Spectral Intensity Distribution	28
Figure 3.20:	Raspberry Pi Pico Pinout Diagram	29
Figure 3.21:	Flow Diagram of Data Collection	30
Figure 4.1:	Prototype Design	31
Figure 4.2:	Response of Drop Test (12m sensor)	32
Figure 4.3:	Response of Drop Test (6m sensor)	33
Figure 4.4:	Response of Drop Test (10m sensor)	33
Figure 4.5:	Saturation of 12m Sensor	34
Figure 4.6:	Speaker Test	35
Figure 4.7:	Waveform of Speaker Test (Red: function generator, Blue: sensor)	36
Figure 4.8:	Frequency Domain of the Response when Speaker is Turned Off	37
Figure 4.9:	Frequency Domain of the Response when Speaker is Turned to 8 kHz	37
Figure 4.10:	Frequency Domain of the Response when Speaker is Turned to 20 kHz	38
Figure 4.11:	Normal Condition Data	38
Figure 4.12:	Segmented Data	39
Figure 4.13:	Wavelet Transformed Data	39
Figure 4.14:	Signal Multiresolution Analyzer	40
Figure 4.15:	Denoised Data	40
Figure 4.16:	FFT of Denoised Data	41
Figure 4.17:	Flow Diagram of Signal Processing	41
Figure 4.18:	Time Domain Data	42
Figure 4.19:	9 th Segmented Data from Normal Condition Data	43

Figure 4.20: FFT of Data	43
Figure 4.21: Time Domain Data of Weighted Condition	45
Figure 4.22: Frequency Domain Data of Weighted Condition	45
Figure 4.23: Time Domain Data of Obstacles Condition	46
Figure 4.24: Frequency Domain Data of Obstacles Condition	46

LIST OF SYMBOLS / ABBREVIATIONS

ADC	Analog to digital converter
AOM	Acoustic-Optic modulation
APC	angled physical contact
ASE	Amplified spontaneous emission
CSV	Comma-separated value
CW	Continuous wave
EAM	Electro-Absorption modulation
EDF	Erbium doped fiber
EDFL	Erbium doped fiber laser
EOM	Electro-Optic modulation
ETS	Electric train service
FBG	Fiber Bragg grating
FC	Fiber-optic connector
FFT	Fast Fourier transform
FPI	Fabry-Perot interferometer
GP	General purpose
IDE	Integrated development environment
KTM	Keretapi Tanah Melayu
LRT	Light rail transit
MRT	Mass rapid transit
MZI	Mach-Zehnder interferometer
NDT	non-destructive testing
OM	Optical microphone
OSA	Optical Spectrum Analyzer
PC	physical contact
SD	Secure digital
SMF	Single mode fiber
SNR	Signal-to-Noise ratio
USB	Universal serial bus
WDM	Wavelength division multiplexing

LIST OF APPENDICES

Appendix A: Pigtailed Laser Diode Specification Sheet	34
Appendix A: Photodiode FGA01FC specification sheet	36

CHAPTER 1

INTRODUCTION

1.1 Railway System in Malaysia

Railway is a significant component of land transports. There are many advantages using a railway system, such as cost-effectiveness, organization, large capacity, high speed over long distance, etc. With these advantages, a railway system is utilized in both passenger and freight transportation. Globally, railway systems are widespread with extensive networks in many countries. Among these countries, USA, China and Russia are the countries that constitute the majority of the railway network (James, 2023).

The Land Public Transport Agency (Agensi Pengangkutan Awam Darat (APAD)) (2024) reported that in Malaysia, there are 11 types of train systems including both freight railway and passenger railway. These railways are monorail, Mass Rapid Transit (MRT), KLIA aerotrain, KTM intercity, Electric Train Service (ETS), KTM Commuter, Skypark link, KTM Cargo, KLIA Express, KLIA Transit and Light Rail Transit (LRT). The total length of railway transport is about 2783 km, most of it is Keretapi Tanah Melayu (KTM) operated by Keretapi Tanah Melayu Berhad (KTMB) with the total length of 1641 km. It is utilized in freight transport and commuter rail service. The remaining part of the railway system are the passenger trains, operated by RAPIDKL and PRASARANA.

Table 1.1: Number of Passengers for Rail Transport Services, 2023

	First Quarter	Second Quarter	Third Quarter	Fourth Quarter	2023
Ampang Line	12,244,799	11,577,226	13,001,834	13,766,720	50,590,579
Kelana Jaya Line	17,304,965	17,408,097	19,115,670	19,934,860	73,763,592
Monorail Line	4,099,687	4,271,287	4,628,078	5,108,521	18,107,573
MRT Kajang Line	14,475,889	15,757,999	17,247,227	19,020,393	66,501,508
MRT Putrajaya Line	3,218,613	7,223,564	8,868,780	10,244,894	29,555,851
KLIA Express	312,275	334,583	388,436	405,479	1,440,773
KLIA Transit	1,247,862	1,214,673	1,318,395	1,362,443	5,143,373
Total	52,904,090	57,787,429	64,568,420	69,843,310	245,103,249

SUMBER Source: PRASARANA MALAYSIA BERHAD, EXPRESS RAIL LINK SDN.BHD

Table 1.1 shows the number of passengers for rail transport services in 2023. In the statistics report by the Ministry of Transport Malaysia (2024), there are total 245, 103, 249 passengers who take the LRT, MRT, KLIA Express and

KLIA Transit in 2023. Although the railway system is well-developed and mature, there have still been many suspected cases of railway accidents or incidents around the world in the last few decades. In Malaysia, a significant railway accident occurred in May 2021. This incident involved a collision between a train carrying 213 passengers and an autonomously driven test train in a tunnel situated between the Kampung Baru and KLCC stations. The accident resulted in serious injuries for 47 passengers, with 6 of them requiring admission to an intensive care unit. Additionally, 166 passengers sustained minor injuries (Chin, 2021).

1.2 Existing Sensors for Detecting Railway Defects and Tracks Irregularities

Recent studies by Shahrir and Manan (2021) have identified several factors contributing to these tragic accidents. Collision is the major cause, accounting for 52.63% of the accidents. This is followed by derailment, which contributes to 15.73% of the accident. Gap fall make up 10.53%, while mechanical failure, being scraped by train, and fire each account for 5.26% of the accidents as shown in Figure 1.1.

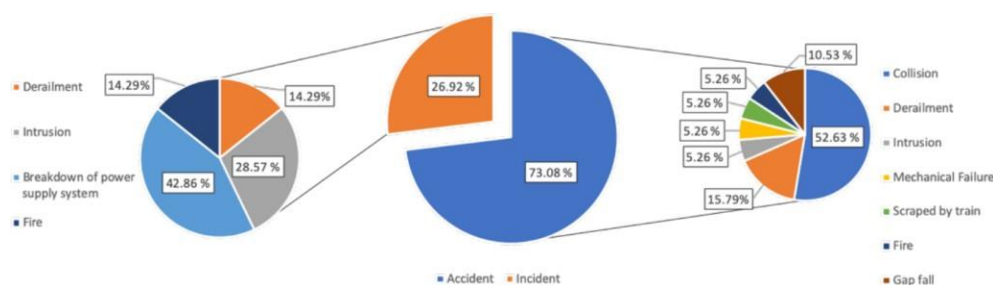


Figure 1.1: Factors contributing to the rail accidents and incidents in Malaysia (Shahrir and Manan, 2021)

Most of the factors are caused by human error which can be reduced by automate the railway and train control by computer system. The reduction of derailment and failure of equipment can be achieved through the enhancement of sensors system or method used for detecting railway defects and the improvement of the railway health monitoring system.

The traditional method of rail defect detection has been human manual inspection. However, the use of railway is increased in recent years and the trend is expected to continue rise in the future, train density, running speed, load

capacity has increased rapidly, especially in high-speed rail transportation. Railway health detection method must be upgraded and automated to handle the large network of railway system. At present, a variety of non-destructive testing (NDT) methodologies are employed to the field of railway inspection. These methods include, but not limited to, visual inspection, ultrasonic testing, eddy current testing, magnetic flux leakage detection, alternating current field measurement, Barkhausen noise analysis, acoustic emission technology. These NDTs are effective in identifying potential issues of the railway without causing damage to the structure (Gong et al., 2022).

These sensing methods are effective in respective field but they are also limited to some factors. Visual inspection method required high-definition video, unable to detect internal defects and is limited to the light changes of the environment is causing issue to the result of the inspection (Singh et al., 2017). Ultrasonic testing inspection speed is low, it cannot be used in long-distance detection as it required a coupling agent during the inspection and the method is difficult to detect rail defects with complex shapes (Ge et al., 2021).

Electromagnetic sensors such as eddy current, magnetic flux leakage, alternating current field measurement and barkhausen noise are very effective in surface and near surface defects detection and high response speed. Still, these electromagnetic sensors are highly sensitive to electromagnetic field, consequently these sensors need to consider the electromagnetic interference when applied (Mathur and Raman, 2020). Besides that, electromagnetic sensors required stable power supplies to be functional on-site.

1.3 Fiber Optic Sensors in Railway Monitoring

Fiber optic sensors, known for their high sensitivity, immunity to electromagnetic interference, low signal loss in long distances have become prevalent in various field of studies (Du et al., 2020). In recent years, fiber optic sensors have been recognized as potential technologies for railway monitoring as their accuracy and reliability in measuring various physicals parameters such as temperature, vibration, strain, in real-time.

Among these physical parameters, vibration presents an intriguing area of study in railway monitoring. Therefore, a vibration sensor serves as an effective tool for detecting and measuring vibrations induced by passing trains.

Fiber optic sensors are sensitive in capturing the vibrations including acoustic vibration. In railway health monitoring, these sensors are able to detect track defects, cracks, fractures or deformations. There are several methods in utilizing fiber optic sensor in railway monitoring, included but not limited to grating-based sensors such as fiber Bragg grating (FBG) (Filograno et al, 2011), interferometry-based sensors such as Mach-Zehnder interferometer (MZI) and Fabry-Perot interferometer (FPI) (Dandridge, A., 2011) and fiber optic distributed acoustic sensing interrogator etc (Kowarik et al., 2020).

1.4 Problem Statement

In contrast to the full implementation of real-time monitoring using fiber optic sensors in neighboring countries, Malaysia's current railway health monitoring and inspection methods still rely on the traditional sensors for static monitoring.

Even though the current systems work to some degree, they are limited to provide real-time insights into track conditions. Traditional systems operate on a schedule, conducting inspections at predetermined intervals, it might lead to delayed detection of defects. If the current state of the railway health monitoring system persists without change, it could potentially compromise passenger safety, and performance and capacity are not optimized.

A different approach of railway health monitoring is proposed. In this project, we investigate the possibilities and effectiveness of a fiber optic acoustic sensor in railway health monitoring. Laser dynamics fiber sensor with Erbium Doped Fiber Laser (EDFL) is used to monitor the acoustic waves and vibration of the infrastructure.

1.5 Aims and Objectives

- 1) To investigate the feasibility of using fiber lasers for detecting and picking up acoustic and vibration signals generated during train operation and to identify the key laser dynamics behavior that allows for the detection of such signals.
- 2) To design and build a portable fiber laser sensor that can interact with acoustic waves and vibration.
- 3) To compare and evaluate different signal processing techniques and noise filtering algorithms for their effectiveness in detecting and monitoring acoustic signals and vibrations detected by fiber lasers.

1.6 Project Scope

This project introduces an alternative method where a laser dynamics fiber sensor is proposed to monitor the vibration and acoustic waves of the train structure during operation. Fiber optic sensors are attached to the train of the mock railway system to collect the vibration signals. The mock railway track is 36 m long.

The sensors can be divided into three parts: the laser source, the fiber sensor, and the data collecting module. The laser source and the data collecting module require a power source of 5V, so power banks with USB-C cables are used. A Raspberry Pi Pico, which is a microcontroller, is utilized with a micro-SD card reader to collect the acoustic vibration signal and store it in the micro-SD card for data analysis.

The Micro Python IDE, Thonny, is used to program the microcontroller. PicoScope 7 T&M software is used in the study of the behavior between the vibrations and laser dynamics. MATLAB is used for data analysis and machine learning.

The sensors utilize laser dynamics behavior for sensing and monitoring. In the early stage of the project, a 980 nm laser pump, a photodiode, a digital oscilloscope, and different fiber optic sensors are used to study the laser dynamics characteristics. In the second stage, a prototype will be designed with mounting holes to attach to the simulated train of the railway. In the third stage,

data will be collected from the mock railway system. In the final stage, the work will focus on signal processing and data analysis.

The project outcomes are limited to the mock railway system. The designed prototype requires micro-SD card to collect the data. Therefore, the health monitoring system is not real-time monitoring in this project. Data collected need further processes before it shows any useful results. Automation and modification on data collection and data analysis are additional features that can be included in later increments of the project.

1.7 Outline of the Report

This paper is structured as follows: Chapter 2: Literature Review discusses the theory of EDFL and laser dynamics characteristics that are of interest in acoustic vibration sensors, specifications of optical components, data collecting methods, sensor packaging, and fundamental machine learning approaches in data analysis. Chapter 3: Methodology and Working Plan discusses the work plan and the procedure for setting up the sensors and collecting data. Chapter 4: Results and Discussion presents the observations and results collected throughout the project and discusses and analyses the data collected. Chapter 5: Conclusion and Recommendations concludes the report and provides recommendations based on the outcomes of the project

CHAPTER 2

LITERATURE REVIEW

2.1 Theory

2.1.1 Stimulated Emission and Population Inversion

When a photon with energy, $E_p = h\nu$, is absorbed by an electron in an atom, the electron will be excited to a higher level, E_2 , from initial energy level, E_1 . The electron in higher energy level emits a photon and transit down to a lower unoccupied energy level. There are two possibilities for the photon emission process which is spontaneous emission and stimulated emission.

$$E_p = E_2 - E_1 \quad (2.1)$$

where

E_p is the energy of the photon

h is the Plank's constant

ν is the frequency of the photon

In spontaneous emission, electron undergo downward transition from E_2 to E_1 and emits a photon of energy $h\nu = E_2 - E_1$ in random direction. The excited electron spontaneously decays to the ground level over a period of time. The emitted photon is incoherent in phase and generate a broad spectral width.

In stimulated emission, an incoming photon of energy $h\nu = E_2 - E_1$ stimulates the emission process by inducing the electron at E_2 to transit down to E_1 (Kasap, 2013). The emitted photons have the same energy, polarization and direction with the incoming photons.

When there are enough atoms at E_2 , more than atoms at E_1 , population inversion is achieved. Population inversion can only achieve when there are more than 2 energy levels, as if there are only 2 energy levels, the incoming photons will cause as many upward excitations as downward stimulated emissions.

Figure 2.1 shows the concept of absorption, spontaneous emission and stimulated emission in energy band diagram

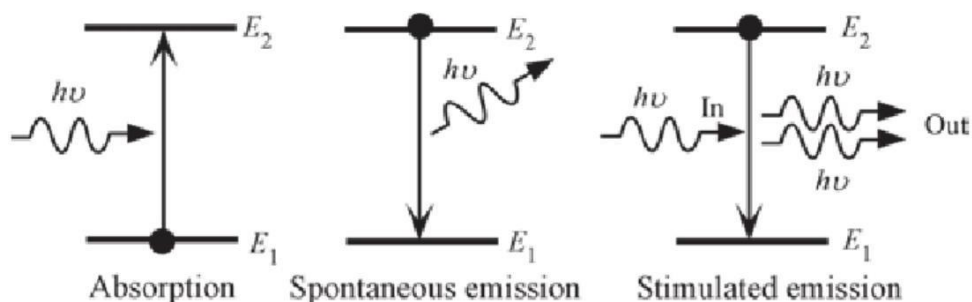


Figure 2.1: (a) Absorption (b) Spontaneous emission, and (c) Stimulated emission(Kasap, 2013)

2.1.2 Laser Principle

Consider a three-energy level system (E_1 , E_2 , E_3), suppose that an external excitation causes electrons at ground energy, E_1 to excite to higher energy (E_3). This excitation energy is called pump energy, the process is called optical pumping with a source (photons) with certain wavelength that can be absorbed by the laser medium.

The electrons that are excited to the higher level, E_3 decay rapidly to lower energy level, E_2 and emit phonons (heat) as the transition energy is not sufficient to emits photons and stay in E_2 as it is the energy level where electrons do not rapidly decay to the ground state. Excited electrons will accumulate at E_2 and hence population inversion between E_2 and E_1 is achieved.

When electrons at E_2 decays spontaneously, it emits photons that stimulate neighboring electron at E_2 to emits photons (stimulated emission), this process go on and caused avalanche effect of stimulated emission where all the photons emitted are in phase, in same direction and polarization. The emission process of the coherent light (photons) is called lasing emission (Hecht, 2019).

After all excited electron dropped to ground energy level, the electrons can be pumped again to repeat the processes. Figure 2.2 displayed the energy band diagram of Erbium Doped Fiber.

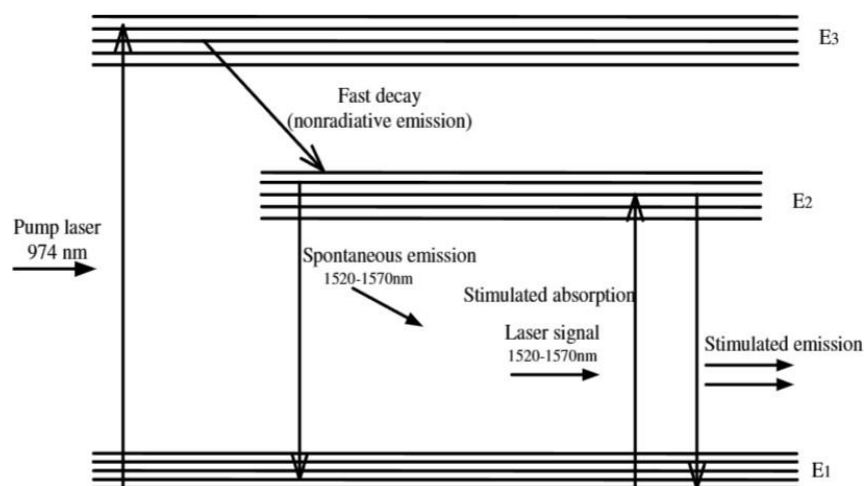


Figure 2.2: Simplified Energy levels of Er³⁺ ions in Erbium-doped fiber (Zhu, Li, and Helmy, 2007)

2.1.3 Fiber Optics

Fiber optics are long thin fibers of glass (silica) or plastics (polymers) that guide light along their length. Similar to wires, fiber optics are used to transmit signals over distances, but with lower loss, and the transmitted signal is an optical signal. These fibers are flexible, making them useful in many fields such as telecommunications and sensing (Hecht, 2019).

The simplest structure of fiber optics includes the core and the cladding, which are materials with different refractive indices. The fibers are well engineered and manufactured that the transmitted signal (light) is guided within the core of the fibers. The core of the fiber is usually much smaller compared to the cladding. As reference, a single-mode fiber (SMF) has the cladding with diameter of 125 μm and core diameter of only 9 μm . The diameters of the cladding and core determine the mode of transmission of the fiber optics. There is a variety of fiber optics designed in order to suit different functions such as single-mode fiber, step index multimode fiber, graded index multimode fiber etc. to transit different optical signals and active fiber that amplify, generate or modify laser that is transmitted inside the fiber.

Fiber optics, are cost-effective and easy to apply due to their small size and light weight. Secondly, their flexibility enhances usability, making them ideal for various applications. Last but not least, they are immune to

electromagnetic interference and corrosion, which ensures their longevity of use (Rashid and Lovely Yesmin, 2001).

2.1.4 Erbium Doped Fiber Laser (EDFL)

Fiber lasers are solid-state lasers in which laser medium is in the form of an optical fiber. By adding light-emitting elements into glass, optical fiber can be treated as a gain cavity of laser. These fibers are usually doped with rare-earth elements such as erbium, ytterbium, neodymium etc.

Erbium Doped Fiber (EDF) is the most common fiber in constructing fiber laser especially used in broadband optical networks and CATV applications. The core of the fiber is doped with rare-earth element, Erbium (Er), Er^{3+} ions in EDFL are excited by 980 nm or 1480 nm laser and emit 1550 nm laser. In this project, EDF is used as gain medium with the semiconductor laser pump of 980 nm laser. 980 nm is chosen due to its low noise figure, WDM compatibility, suitable to operate at low power (< 20 mW). EDF is spooled into a ring to act as laser resonator in this project. Figure 2.3 shows the example of configuration of ring laser using EDF.

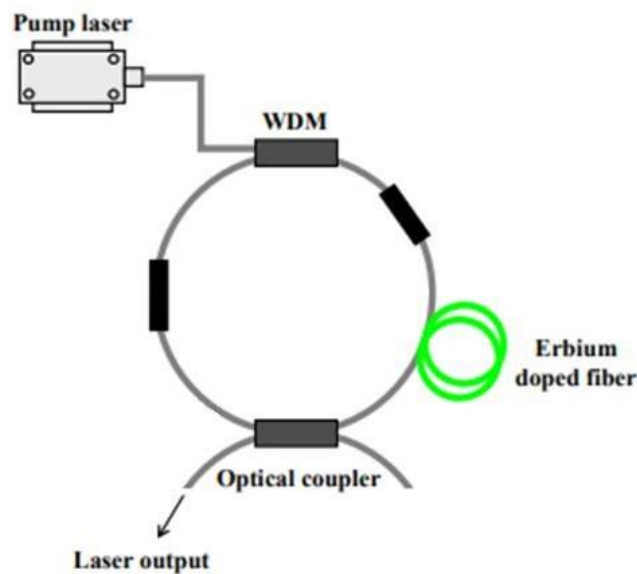


Figure 2.3: Ring cavity of EDFL (Causado-Buelvas, Gomez-Cardona and Torres, 2011)

Additionally, the benefits of EDFL include the extended interaction length between the pump light and the active ions, low coupling loss resulting in high gain. Moreover, they can operate in a single transverse mode, which is achieved by appropriately selecting the fiber parameters. Last but not least, past researchers found that these lasers are very sensitive to perturbation that destabilize the laser signal (Pisarchik et al., 2005), making it a good option in sensor applications.

2.2 Working Principle

2.2.1 Laser Dynamics in EDFL

When the laser is pumped with sufficient power, the lasing system is in an unstable condition that cause laser instability and chaos. The dynamic behavior of laser is studied in past research papers, the instabilities and chaos nature of laser system attracts the interest of scientists. They discovered that the intracavity laser power can grow or decay exponentially toward the difference between gain and resonator losses (Paschotta, 2007). The laser dynamics of EDFL can be described with the following equations (Erneux and Glorieux, 2010).

$$\frac{dI}{dt} = I(-k + gD) \quad (2.2)$$

$$\frac{dD}{dt} = -(1 + I_P + 2I)D + I_P - 1 \quad (2.3)$$

where the symbols are as defined in Table 2.1.

Table 2.1: Symbols from the laser dynamics and their definition

Symbol	Definition
<i>I</i> and <i>I_P</i>	intensity of laser and pump
<i>D</i>	inverted population
<i>k</i>	decay rate of laser
<i>g</i>	unsaturated gain of laser
The above parameters are link to the rate equations parameter as:	
$\mathbf{k} \equiv \frac{\gamma_c}{\Gamma_{21}}, \mathbf{g} \equiv \frac{\sigma_S N_T}{\Gamma_{21}}, \mathbf{D} \equiv \frac{N}{N_T}, \mathbf{I}_P \equiv \frac{\varphi_P \sigma_P}{\Gamma_{21}}, \mathbf{I} \equiv \frac{\varphi_S \sigma_S}{\Gamma_{21}} \text{ and } \mathbf{t} \equiv T\Gamma_{21}$	

N	population inversion ($N_2 - N_1$)
N_T	total Er ions
γ_c	cavity decay rate
φ_P and φ_S	number of pump and incident light photons
σ_P and σ_S	absorption and stimulated emission coefficient of pump and signal
Γ_{21}	spontaneous transition probability of Er ions from level 2 to level 1

Pua, Chong and Ahmad (2013) conducted a simple numerical simulation using equation (2.2) and (2.3). By changing the pump power, I_P , the simulation results show the optical output power fluctuates at the onset of laser action by producing a series of spikes that drops exponentially and return to stable condition. This phenomenon is named as Turn-On Transient in *Laser Dynamics* by Erneux and Glorieux (2010). Other similar transient effects are also simulated by adjusting the decay constant, k . In practical, decay constant is alternated by inducing loss to the laser cavity through external disturbances. Vibration is one of the external forces that cause cavity loss of fiber by inducing periodic refractive index perturbation. Figure 2.4 shows the result of simulation.

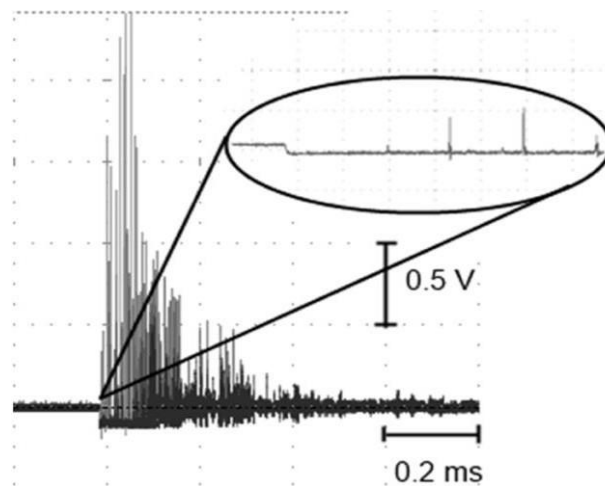


Figure 2.4: Simulation of Optical Power Fluctuation after an impact (Pua, Chong and Ahmad, 2013)

They concluded that when the EDFL is functioning slightly above threshold condition, sudden increase of k value will suppress the lasing effect, consequently reduces the optical output power.

The dynamics behavior of laser is utilized in past researches (Pua et al., 2011) to propose a non-membrane optical microphone (OM). The setup is simple as it consists only a 3 m EDF that is pumped by a 980 nm laser diode with power up to 160 mW, a wavelength division multiplexing (WDM) coupler to combine laser signals with a 25 km conventional single mode fiber (SMF).

The EDF generates amplified spontaneous emission (ASE) in the C-band region (around 1550 nm) when pumped at 980 nm. The 1550 nm port of the WDM coupler is unconnected and cleaved at 90° to act as mirror of the cavity to provide 4% Fresnel reflection. The other end of the setup, the SMF is also left unconnected for the same function. The 2 ‘mirrors’ form a linear cavity in between; laser conditions are fulfilled. Figure 2.5 demonstrates the experiment set up by Pua.

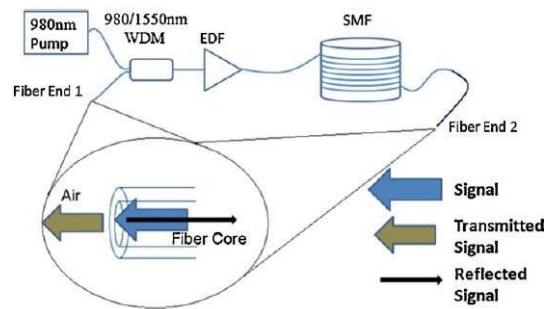


Figure 2.5: Illustration of optical microphone experiment setup (Pua et al., 2011)

The experiment is conducted in several conditions, such as presence of acoustic waves and different pumping power. The experiment demonstrated that external disturbances such as acoustic waves can cause phase shifts of the longitudinal mode and reduce lasing due to mode competition. Multiple-mode competition will cause random self-lasing and leads to small, but rapid, fluctuations in the total optical output power. This is because compression and rarefaction of the acoustic wave cause changes of the refractive index of the fiber. Consequently, the optical signal alters with the acoustic waves, this makes it a highly sensitive and fast response sensor.

As an application of this dynamic behavior of laser, optical signal can carry same information as carried in the acoustic waves (Pua et al., 2011). By comparing the results with normal electrical microphones, the responses of OM are much higher. Figure 2.6 shows the output waveforms.

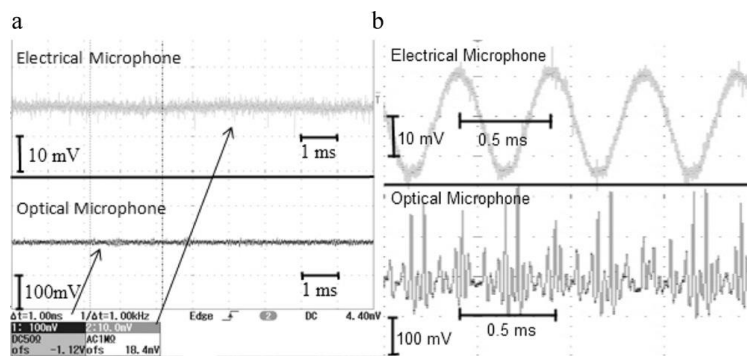


Figure 2.6: Comparison of (a) background noise without acoustic signal (b) with 2 kHz of acoustic signal between electrical and optical microphones (Pua et al., 2011).

Furthermore, a sinusoidal modulation signal is captured from the output waveform of electrical microphones, but there are random spikes against time instead of modulation signal obtained in the output waveform of OM. This is the result showing that OM possessed higher sensitivity compared to electrical microphones. In other words, optical approach is a valuable alternative method to utilize in sensing applications.

2.2.2 Loss Modulation

Past research had demonstrated the sensing mechanism of EDFL system by loss modulation (Woon et al., 2018). When acoustic vibration absorbed by the sensing laser, loss modulation in the lasing cavity will take place, intensity of the laser is modulated by the acoustic waves, causing fluctuation in the output power. Figure 2.7 shows the loss modulation of the EDFL output.

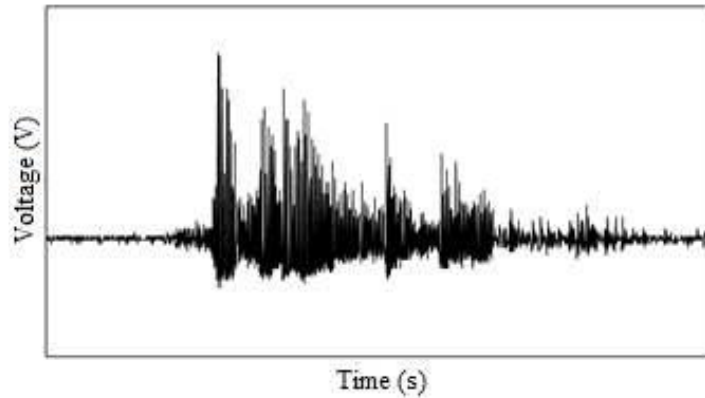


Figure 2.7: Loss modulation behavior of EDFL sensor (Woon et al., 2018)

Laser modulation is process that control an optical wave output and encode information on the transmitted optical signal. Many laser applications require modulation of laser output power especially in fiber-optic communication system. Modulation can happen in two ways, direct modulation that altered the signal before it reaches the laser and external modulation that modulate the signal on the laser system causing laser signal carries information.

In acoustic sensors, external modulation is applied. There are three main continuous wave (CW) output laser modulating techniques such as Electro-Optic Modulation (EOM), Electro-Absorption Modulation (EAM) and Acoustic-Optic Modulation (AOM). This project demonstrates AOM. In AOM, the sensing fiber's refractive index is manipulated by acoustic waves from mechanical vibration and induces loss in the cavity to perform loss modulation.

CHAPTER 3

METHODOLOGY AND WORK PLAN

3.1 Working Plan

In this subchapter, the overall methodology will be discussed, including design of prototype, data collection and signal processing.

3.1.1 Stage 1: Study on the EDFL sensor

- 1) EDFL working principle is studied using old modules as experimented setup in the lab. Figure 3.1 shows the experimental setup. Where (1) is the fiber sensor, (2) is the laser source module, (3) is the photodetector, and (4) is the PicoScope.

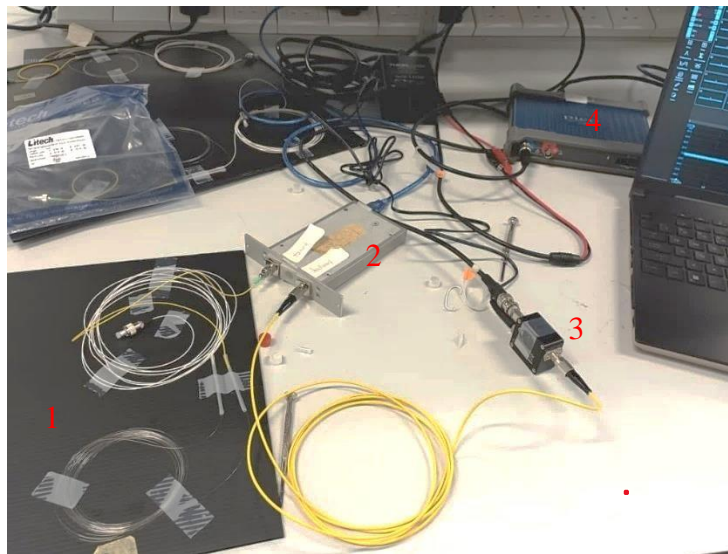


Figure 3.1: Experimental setup of the EDFL acoustic sensor

- 2) The experimental setup included:
 - I. A laser source module with a 980 nm butterfly pinned laser diode, a 3 m EDF spooled into a ring of diameter 4 cm and a WDM coupler that connects 1550 nm and 980 nm inside the case of the module. Figure 3.2 shows the laser source module. Figure 3.3 shows the WDM coupler.



Figure 3.2: Laser Source Module



Figure 3.3: WDM

- II. A photodetector (THORLABS, DET08CFC/M) to capture the output signal. Figure 3.4 shows the photodetector.



Figure 3.4: Photodetector (THORLABS, DET08CFC/M)

- III. A Picoscope 3000 series as digital oscilloscope for data collection and signal analysis. Figure 3.5 shows the PicoScope.



Figure 3.5: PicoScope 3000 series

- IV. A DC power supply to power up every component.

3) There are 2 fiber-optic connector (FC) ports on the laser source module:

- I. Forward, that spliced to EDF, is connected to bare optical fiber with angled physical contact (APC) as sensor.
 - II. Backward that spliced to WDM, is connected to the photodetector with a physical contact (PC) fiber
- 4) The output spectrum is tested and studied with the Optical Spectrum Analyzer (OSA). Figure 3.6 shows the OSA. Figure 3.7 shows the OSA results, backward (left), forward (right).

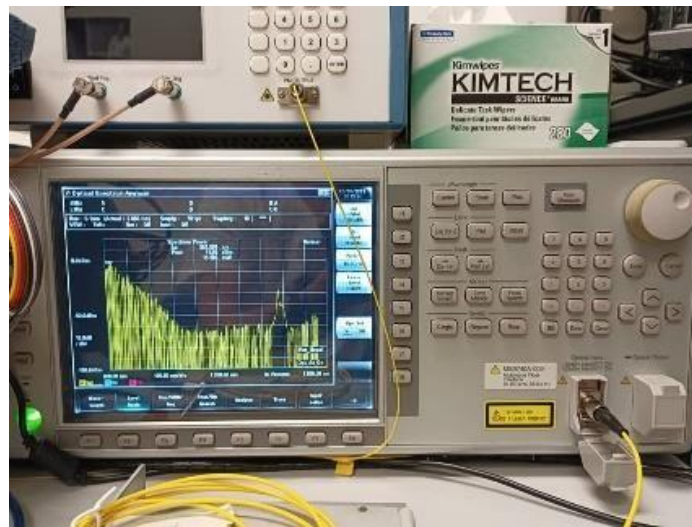


Figure 3.6: Optical Spectrum Analyzer (OSA)

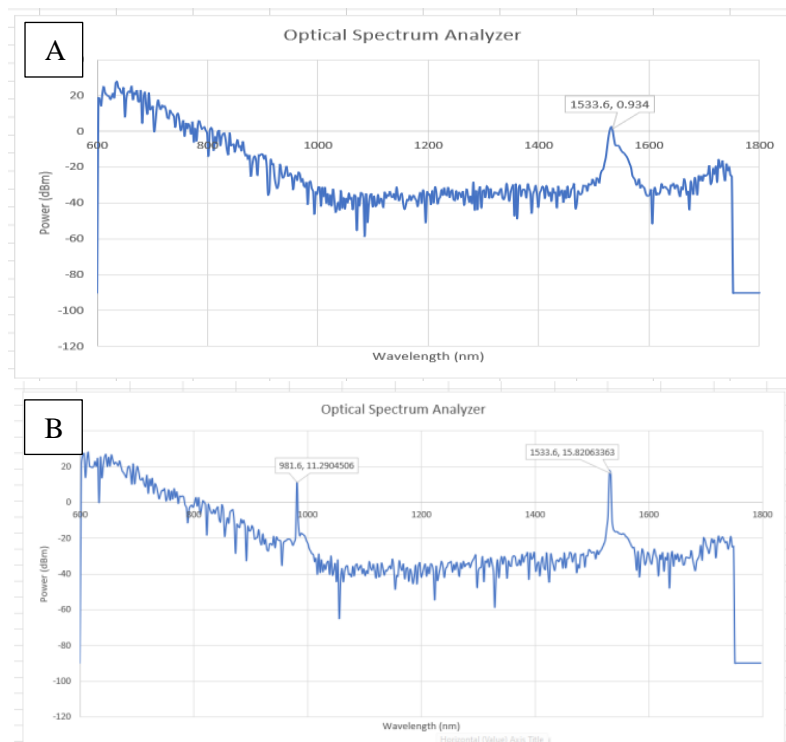


Figure 3.7: OSA results at (A) backward port and (B) forward port

Figure 3.7 shows that backward port contains only 1550 nm signal peak, and forward port contains both 980 nm and 1550 nm signal peaks. 980 nm is generated by the laser source, 1550 nm signal peak is generated by EDF.

- 5) The photodetector is connected to PicoScope with a coaxial cable and then connected to computer with USB cable to collect data in PicoScope 7 T&M software. Figure 3.8 shows the interface of PicoScope 7 T&M software.

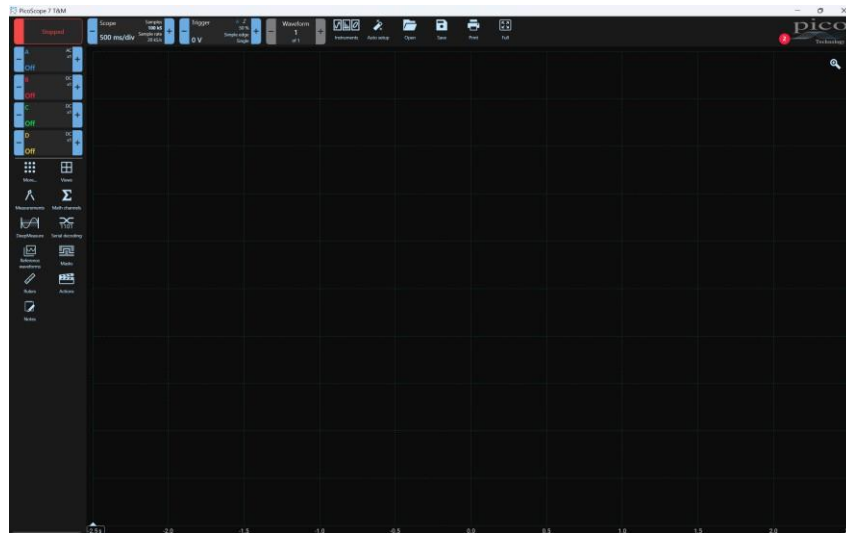


Figure 3.8: PicoScope 7 T&M

- 6) Sensors are built with bare single mode fiber (SMF). Each end of SMF is spliced to PC and APC respectively with splicing tools (fusion splicer, fiber cleaver, fiber stripper). Figures 3.9 show the splicing tools.



(a) Fiber Splicer



(b) Fiber Cleaver



(c) Fiber Stripper

Figures 3.9: Splicing Tools

- 7) Different length of SMF is spooled and stucked on plastic corrugated board from 1 m to 8 m. Figure 3.10 shows different length of SMF spooled into rings.



Figure 3.10: Fiber sensors made of SMF

- 8) Experimental setup is constructed with different length of spooled SMF.
- 9) The setup is tested by tapping on the sensor, plastic board and table and observe the output waveform in PicoScope software. Figure 3.11 shows the output waveform when the sensor is tapped. (Refer to Chapter 4.2, characteristics of the sensor)

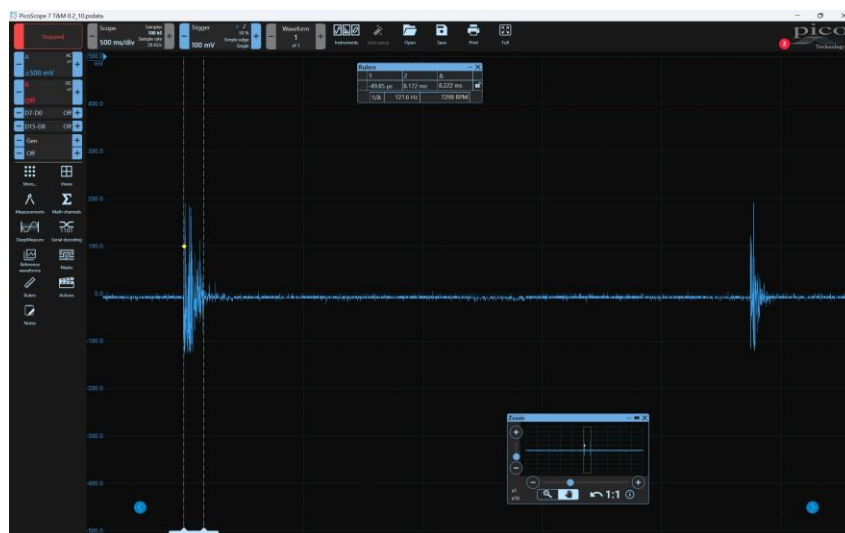


Figure 3.11: Output Waveform in PicoScope when the sensor is tapped

- 10) Speaker test is conducted by placing the sensor on a speaker connected to function generator and observe the output waveform in PicoScope software.

- 11) Testing was done for several times with different sensor length and laser source power.
- 12) Concludes the observation and hypothesis. Record the needed changes.

3.1.2 Stage 2: Design and Build Prototype

The EDFL sensor mechanism is studied in previous subchapter. The prototype contains 3 separated parts, a laser module, sensors and a data collecting module. The laser module contains a laser driver circuit to power up a 980 nm laser diode, a photodiode driver to power up the photodiode, 980/1550 WDM coupler to connect the laser diode, photodiode and sensor.

Sensors are sensing fiber spooled and stick firmly on the plastic sheet. Two patch cords are intentionally separated for some distance with the sensors for easier connection to the laser module. Data collecting module contains a Raspberry Pi Pico microcontroller to collect data from the photodetector and a micro-SD card reader to store the data into micro-SD card for later analysis.

The data collecting module is able to collect data from 4 pins, the output signal of the photodiode is electrical signal that required 2 pins for positive and negative voltages. Therefore, a data collecting module can collect data from 2 sensors and save into a same micro-SD.

Both laser module and data collecting module is 3D printed, the first version is printed with 50 % infill.

3.1.3 Stage 3: Installation and Pre-Testing on Test Bed

The test bed is a mock railway system consist of a 36 m long track and a mock-up train. The track is made of hollow aluminum profiles to simulate real-life railway track. The train consists of 4 wheels, 2 DC motors connected to the rear wheels, rechargeable battery to power up the motors. Figure 3.12 displays the mock railway and the train.



Figure 3.12: Track and Train simulation

Laser module and data collecting module are installed on the train with suitable screws and corner brackets. The laser module is connected with a sensor and the sensor is installed on the aluminum profile above the wheels.

The mock railway system is designed to simulate real-world conditions. As the train is operating, vibrations from the contact of wheels and the tracks and the train body will be captured by the sensors. The optical signal is converted to electrical signal, voltage, by the photodiode and read by Raspberry Pi Pico, and write into the micro-SD card.

Pre testing is performed by operating the sensors and train for 1 minute to test the sensor and try to collect the data. Problem found will be recorded and modification can be performed before data collection.

3.1.4 Stage 4: Data Collection, Signal Processing and Noise Filtering

In this stage of the project, the sensors are operating in good conditions and desired result will be collected.

Normal conditions data need to be collected first with large amount of data set for higher accuracy in future analysis. Different conditions are tested and data is collected including weighted and obstacles.

In signal processing, Fast-Fourier Transform (FFT) is performed in MATLAB to monitor the signal in frequency domain. Noise filtering techniques

are studied and applied in later part to reduce the noise from the system and improve the signal-to-noise ratio (SNR).

3.1.5 Stage 5: Anomalies Detection

This is the final stage of the project, with sufficient data, anomalies detection requires pattern recognition from the large data sets.

Pattern recognition system includes five main phases (Singh, 2023):

- 1) Sensing, convert the input data into analogue data.
- 2) Segmentation, make sure the data is sensed and isolated.
- 3) Feature extraction, recognize the property of the data.
- 4) Classification, categorized the sensed data into a group.

3.2 Prototype Design

3.2.1 Overall Prototype

The laser module and data collecting module is discussed in this subchapter. Laser diode driver circuit is a module bought online and can directly soldered to the laser diode that suit the specifications of the driver. There are 6 pins needed to be connected, VCC and GND are connected to the 2 pin USB-C female port positive and negative respectively. TTL positive pin is shorted to the VCC pin. LD positive and LD negative pins are connected to the positive and negative pin of the 980 nm laser diode. The pin configurations are shown in Figure 3.13.

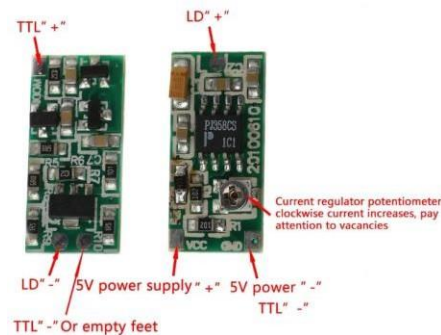


Figure 3.13: Laser Diode Driver

Similar for photodiode, it requires a driver circuit to drive it, oppositely, photodiode have to be driven in reverse bias. Bias voltage of the photodiode circuit is also connected to the USB-C female port positive and negative pins,

parallel to the laser diode driver. A resistor of $1\text{ k}\Omega$ and capacitor of $0.1\text{ }\mu\text{F}$ is connected in the circuit to act as noise filter. A resistor of $10\text{ k}\Omega$ is utilized as the load of the circuit, output voltage is connected in parallel with the load. Figure 3.14 shows the photodiode driver circuit.

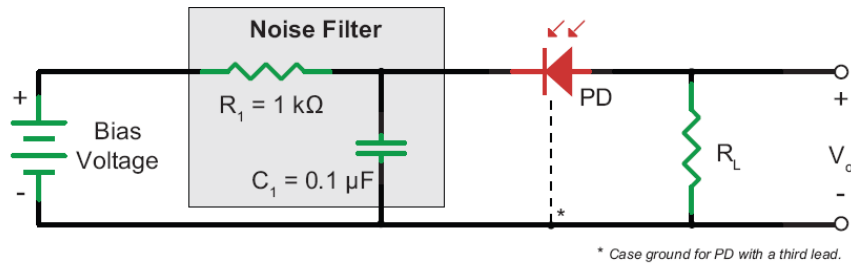


Figure 3.14: Photodiode driver circuit (Thorlabs)

Figure 3.15 shows the overall schematic of the prototype. The circuit is constructed based on the configuration shown in Figure 3.15.

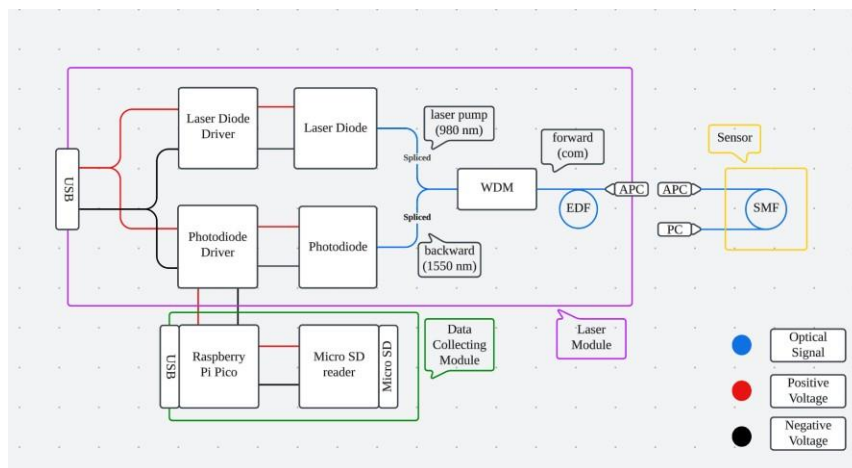


Figure 3.15: Schematic Diagram of the Sensor Prototype

First version of the prototype is constructed using AutoCAD software. Figure 3.16 shows the drawing in AutoCAD software.

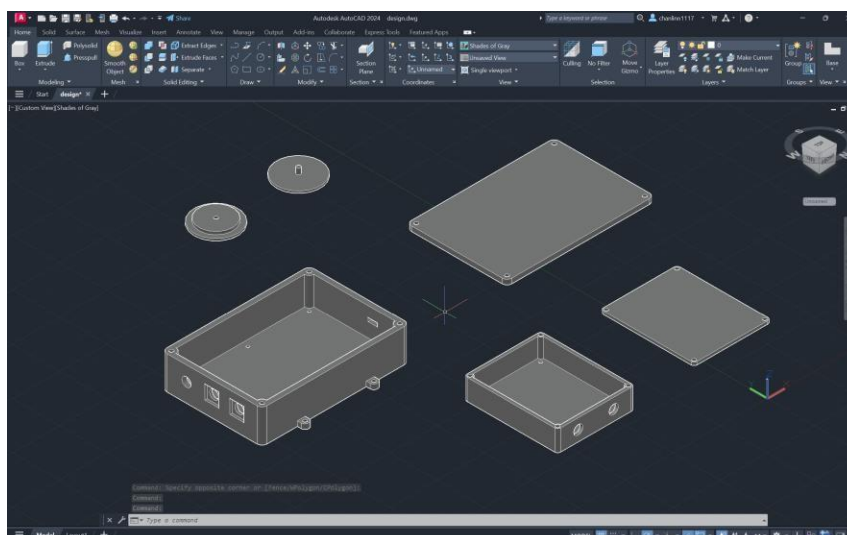


Figure 3.16: AutoCAD Drawing

The drawing included a case for laser module, a case for data collecting module and a circular case to spool the EDF inside the laser module. The modules will be mounted on the train when operating.

3.2.2 Sensor Packaging

Throughout the testing in 3.1.1 subsection, improvements have been done to the sensor design. The SMF is spool nicely side by side on a plastic sheet to achieve maximum contact surface for acoustic vibration. Transducer of the sensor is changed to plastic sheet from plastic corrugated board. This is because plastic sheet is more flexible and thinner compared to the board.

Besides that, it is found that vibrations on the transducer might cause signal loss or noise to the output signal if the sensors are not stick firmly on the transducer material. Therefore, double sided tape is used to hold the fiber between the plastic sheet.

Additionally, patch cords of the SMF are causing additional vibration to the sensors when expose to vibration. This doubt is solved by extending the fiber length to the sensor and leave the patch cords further from the sensor.

Lastly, it was found that the sensors are having large surface area, it is redundant, causing difficulties to install the sensors. To solve this issue, the sensors are spool into circles with inner radius of 4 cm, slightly larger than 3 cm which is the maximum bending of the fiber.

By applying these modifications, the finalized sensor packaging is shown as Figure 3.17.

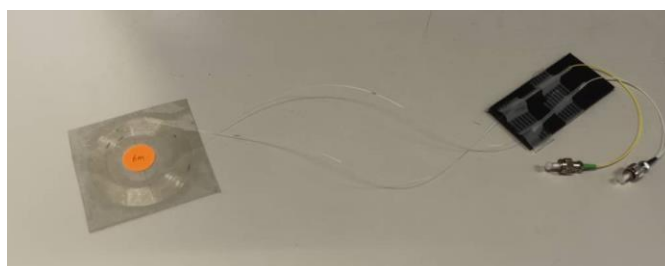


Figure 3.17: Sensor Packaging

3.3 Optical Components

The EDFL acoustic vibration sensors are pumped by a 980 nm laser diode and monitored with a high response photodiode.

3.3.1 Laser Diode

Laser diode used in the project is a 980 nm semiconductor laser diode. The laser is pigtailed with 1 m fiber and connected to the 980 nm port of the WDM. The connector of the laser diode is FC/APC, APC connector is commonly used in optical transmission systems or sensors. These connectors can reduce reflections between fibers connections.

The laser diode is a low power laser diode, it operates below 20 mW with the threshold current of 10 mA. The laser diode used in this project is a 3 pins pigtailed laser diode with single mode core of 9 μm diameter. Figure 3.18 shows the laser diode used in the project. Specifications of the laser diode is prepared in appendix. (Appendix A: Pigtailed Laser Diode Specification Sheet).



Figure 3.18: Pigtailed Laser Diode

3.3.2 Photodiode

In optic fiber based acoustic sensors, a high response high SNR should be achieved for optimum conditions of the sensors. Hence a good photodiode is required. The photodiode that used in this project is an InGaAs high speed photodiode by Thorlabs, the model of the photodiode is FGA01FC.

This photodiode is ideal for both pulsed and CW fiber light sources. The specification sheet of FGA01FC is prepared in appendix (Appendix B: photodiode FGA01FC specification sheet) Figure 3.19 shows the responsivity spectrum of the photodiode.

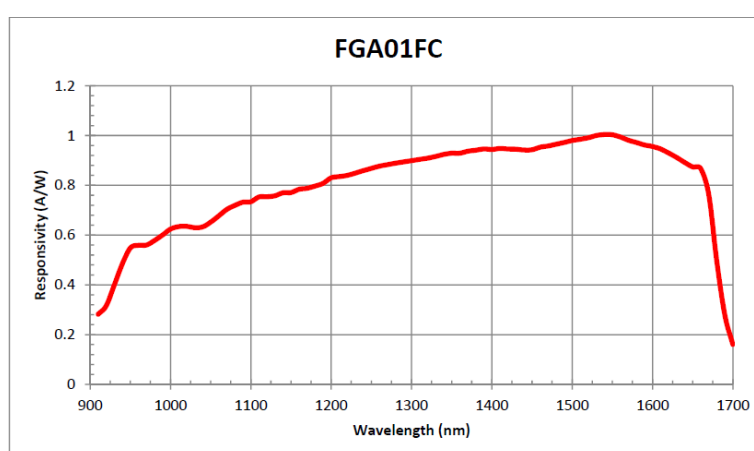


Figure 3.19: Spectral Intensity Distribution

From the graph above, it can be seen that the photodiode has the peak response to 1550 nm light, with responsivity of 1.003 A/W. This wavelength matches the wavelength of the laser emitted by the EDF when pumped with 980 nm. The rise/fall time of the photodiode is 0.3 ns, which indicates an extremely fast response in acoustic sensors. Furthermore, the maximum optical power for the photodiode to operate without damage is 18 mW, which is sufficient for a low-power laser to operate.

3.4 Data Collection

Data collection of the prototype required an oscilloscope to real-time monitoring or devices that can save the data for later analysis. Raspberry Pi Pico is chosen to collect the electrical data from the photodiode and write it in a micro-SD card as CSV files.

3.4.1 Raspberry Pi Pico

Raspberry Pi Pico is a microcontroller from Raspberry Pi, it is a small programmable device that can perform many functions. A Raspberry Pi Pico is utilized as a data logger device. The main function of this microcontroller is to read the voltage signal from the ADC (analogue to digital converter) and write it as CSV in a micro-SD card through a micro-SD card reader module purchased online.

Figure 3.20 shows the pin out diagram of the Pico. 2 ADC is used to read the voltage signal of a sensor. 4 general purpose (GP) pins are used to connect the micro-SD card reader for data logging. Besides that, Vout Pin and GND pin is connected to power up the micro-SD card reader.

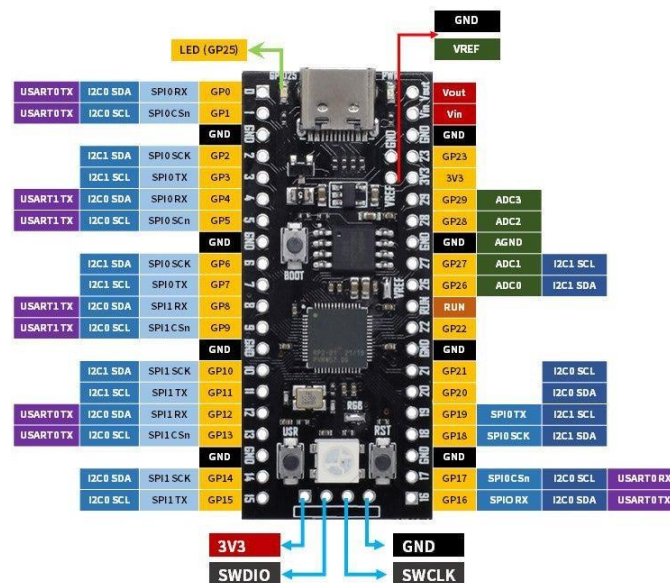


Figure 3.20: Raspberry Pi Pico Pinout Diagram

An Integrated Development Environment (IDE) software is required to program the Pico. Thonny software is used as the IDE of Pico in this project. Pico is easy to use as it operates in MicroPython language, there are many prepared libraries that are useful and convenient such as machine library that allow the user to program the pins for different functions.

A simple code is written in Thonny and saved in Pico as *'main.py'* to operate non-stop when it is powered up. One of the main functions of *'main.py'* is to read voltage fluctuation of the photodiode with 2 ADC pins, positive and

negative pins respectively. Secondly, write the data into micro-SD card. The data is stored as buffer first and flushed into the card for better performance.

The maximum sampling rate of the ADC pins is 500kS/s with the resolution of 12-bit resolution from 0 to 3.3V. These features of Raspberry Pi Pico made it a good data logger for sensor in this project. The performance is outstanding with its cheap cost.

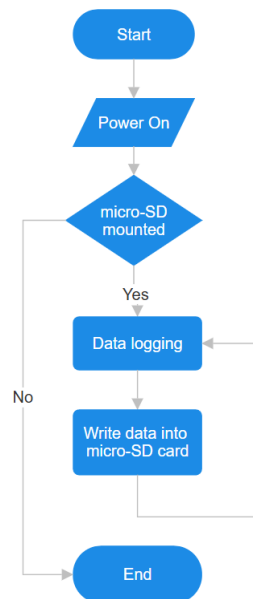


Figure 3.21: Flow Diagram of Data Collection

The above flowchart shows the procedure of the program in Raspberry Pi Pico for data collection. The program is end when power is turned off or micro-SD card is unmounted.

CHAPTER 4

RESULT AND DISCUSSIONS

4.1 Introduction

In this chapter, characteristics of the sensors and results will be presented. Discussions on the results are presented along with the results. Experiment tests are conducted to test the performance of the sensor and the reliability of the design of the sensor system. The sensors are compiled in the laboratory before attached to the mock railway system.

4.2 Fiber Laser Sensor

The finalized fiber laser sensor is built with the idea shown in previous chapters. Figure 4.1 shows the exterior of the fiber laser sensor prototype.

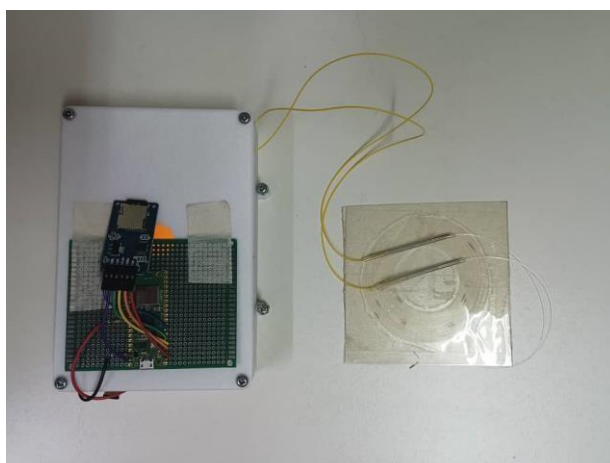


Figure 4.1: Prototype Design

Data collecting module is attached to the cover of the case of the laser source module to minimize the size. Sensors are left outside of the case, to be attached. A micro-SD card is required to save the collected data from the Raspberry Pi Pico. 2 micro-SD cards are prepared for better convenience when collecting data.

4.3 Characteristics of the sensors

4.3.1 Response of sensor in time domain

Before the data are collected, the sensors with different length are tested in the laboratory. The sensors are tested by dropping a weight (screw) with different height. Turn on transient effect of the sensor is observed and investigated. Figure 4.2 shows the response of the sensor in Picoscope software.

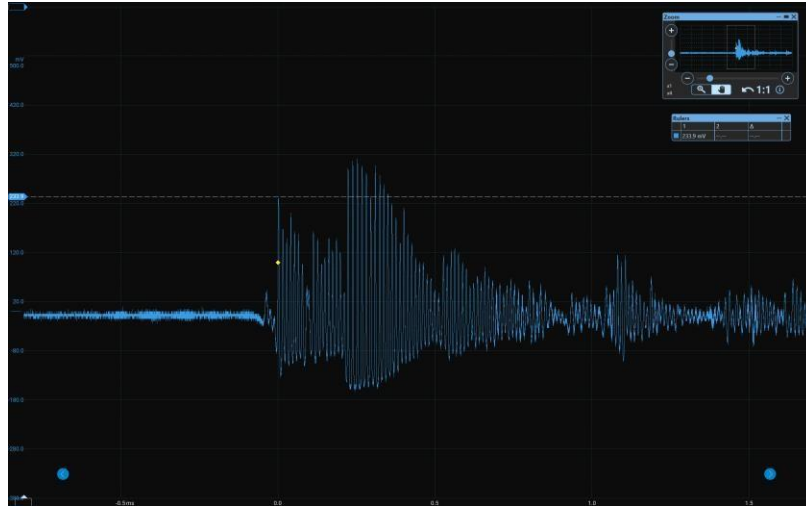


Figure 4.2: Response of Drop Test (12m sensor)

In previous chapter, we discussed about the turn-on-transient effect of laser in laser system, suppression of the laser is a trigger of the sudden huge peak. In the response of the sensors, the suppression is always observed followed by the first peak. There are also multiple packages of peaks with reducing amplitude continuously captured. This periodic change of the signal is due to refractive index perturbation by the vibration in the optic fiber. Figure 4.3 and Figure 4.4 shows the response of different length sensors.

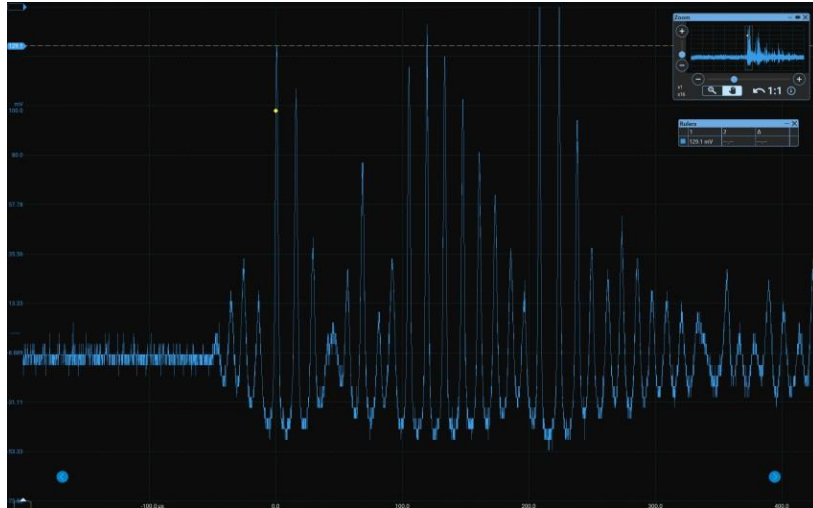


Figure 4.3: Response of Drop Test (6m sensor)

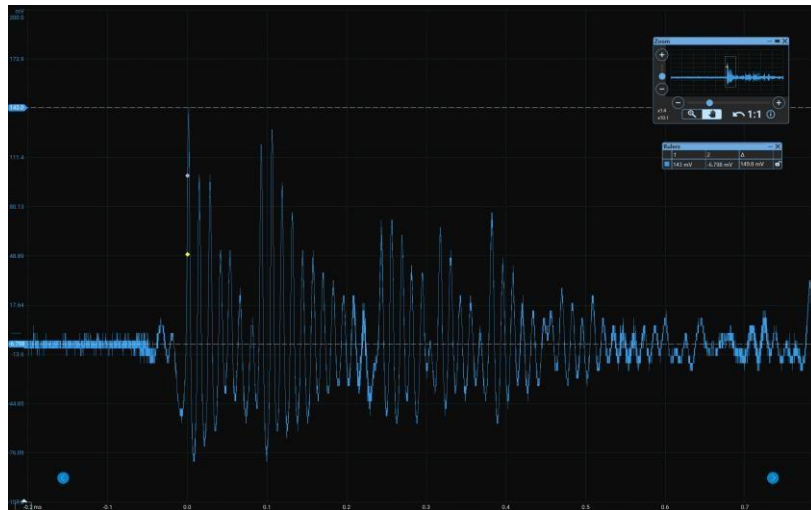


Figure 4.4: Response of Drop Test (10m sensor)

The conducted experiment sets to test the relationship of the length of optic fiber and the response. The sensor is attached on table with double sided tape. A screw is release from constant height, 20 cm and 10 cm away from the center of the sensor. The response is captured with Picoscope. In Figure 4.3, the first peak from 6 m sensor is 129.1 mV, in Figure 4.4, the first peak from the 10m sensor is 143mV. It is then undergone multiple attempts to collect a rather average result. Table 4.1 shows the average value of the first peak of different length sensor from the drop test.

Table 4.1: Table of Peak Amplitude of Sensors with Different Length

Sensor Length (m)	6 m	8 m	10 m	12 m
Amplitude of first peak (mV)	129.1	135.2	231.6	291.3
	110.4	217.7	285.4	288.5
	120.3	144.8	253.7	315.1
	139.1	149.9	221.7	241
	167.2	107.2	200.7	271.4
	114.2	172.6	238.3	305.6
	84.7	114.6	129.3	268.6
Average (mV)	123.57	148.85	222.95	283.07

From the above result, the response of the sensor with different length is investigated. In this section, it is apparent that longer sensor can produce higher peak in average.

Besides that, saturation is also an interesting characteristic of the sensor. When the vibration is large, the suppression of the laser could not produce higher peaks, it would result in a saturation condition in the response. Subsequently, the sensor is tested with heavier weight to measure the saturation of the sensor. Figure 4.5 shows the saturation of the 12m sensor.



Figure 4.5: Saturation of 12m Sensor

The saturation of the sensor is represented in the figure above, at saturation, all peaks are at maximum and decay is hard to observed.

It is known that vibration in further distance will cause minor impact due to the loss of energy, only near distance (10 cm) is tested. Other than that, minor variables such as wind and noise is neglected as the vibration of the train when it is operating will be significantly larger than these factors.

The sensor is then attached to a speaker to test the response of the sensor when constant vibration is applied (acoustic vibration from sound). The experiment is shown in Figure 4.6.

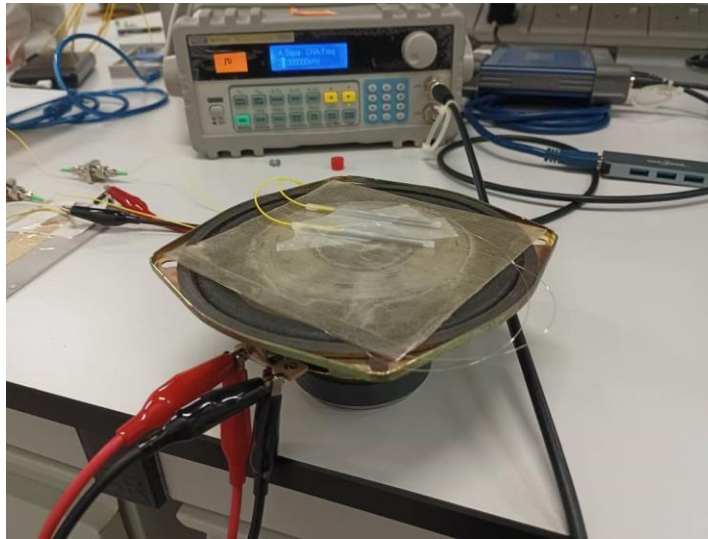


Figure 4.6: Speaker Test

The speaker is attached to a function generator. The response of the sensor and the waveform of the function generator are captured by Picoscope. The input waveform is set to 2.5 kHz. Figure 4.7 shows the waveform captured by Picoscope.



Figure 4.7: Waveform of Speaker Test (Red: function generator, Blue: sensor)

The red waveform represents the output signal of the function generator and the blue waveform represents the output of the sensor. The signal from the function generator is set to 2.5 kHz, however the measured frequency of the sensor output is 2.78 kHz, a slightly different frequency is observed and negligible. The inaccuracy can be considered as systematic error in this case, this phenomenon might cause by the calibration error of the function generator and the oscilloscope.

Aside from that, the waveforms are misaligned, they have a constant phase different of 180° or delayed $179 \mu\text{s}$. The delay is small and can be fixed by calibrating the signal with real time event. Additionally, the delay will be higher when collecting data with Raspberry Pi Pico as the microcontroller takes time to read and write the data into a micro-SD card.

There are several factors that influence the delay in response such as performance of photodiode, memory of the microcontroller, resolution and sampling rate of ADC and the sampling rate of micro-SD reader and capability of the micro-SD card. In this project, the sampling rate is enough with the resolution. The micro-SD card utilized in the project has a capacity of 1 GB is also very sufficient for the sensor to operate.

4.3.2 Response of Sensor in Frequency Domain

The response of signal in frequency domain is also tested by using the same experiment set up with the speaker test. The frequency domain of the sensor response is observed with the spectrum function in Picoscope. Figure 4.8, Figure 4.9 and Figure 4.10 show the spectrum plot when the speaker is turned off, 8 kHz and 20 kHz.

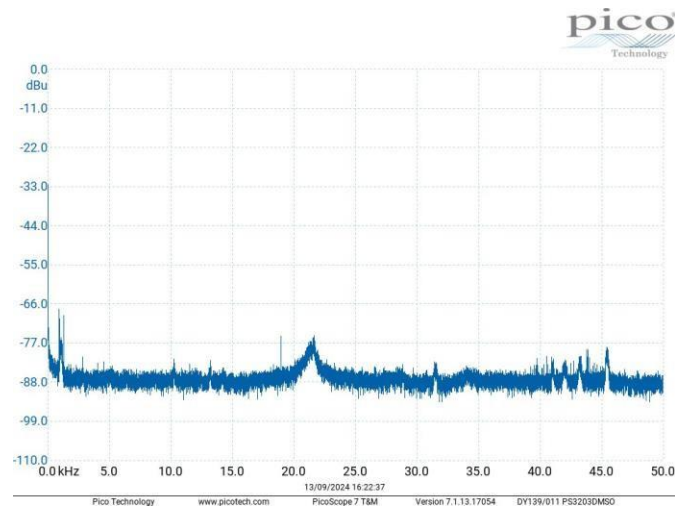


Figure 4.8: Frequency Domain of the Response when Speaker is Turned Off

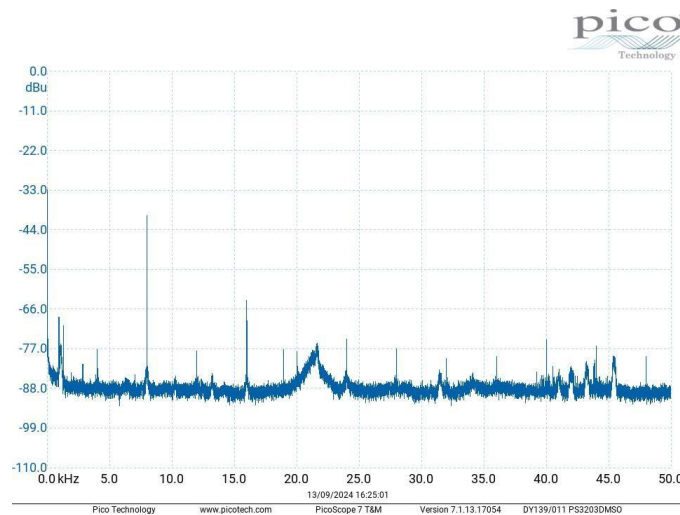


Figure 4.9: Frequency Domain of the Response when Speaker is Turned to 8 kHz

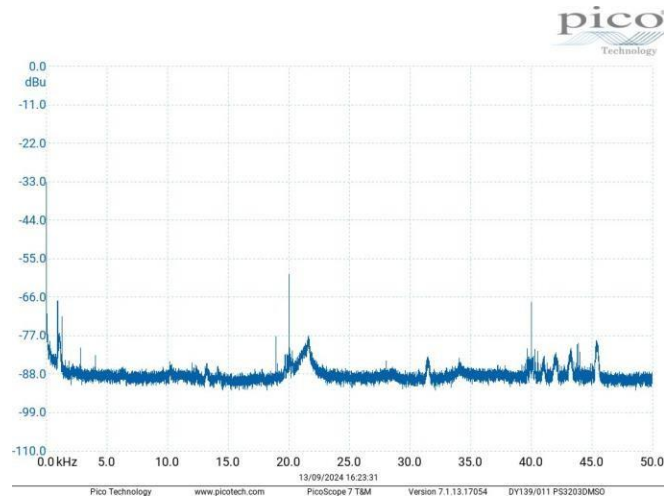


Figure 4.10: Frequency Domain of the Response when Speaker is Turned to 20 kHz

By comparing the results, we observed that there are different peaks when the sensor is exposed to 8 kHz and 20 kHz sound. These peaks are the dominant frequency captured by the sensor when operating in different conditions. With this idea, events can be determined by comparing the frequency domain data of the normal condition and the special condition.

4.4 Data Acquisition

The sensor is attached to the mock train and data is collected. Data are saved in separated files; each file contains 10000 data points with time interval of 10 μ s (100 kS/s). These data are inputted to MATLAB.

4.4.1 Signal Processing

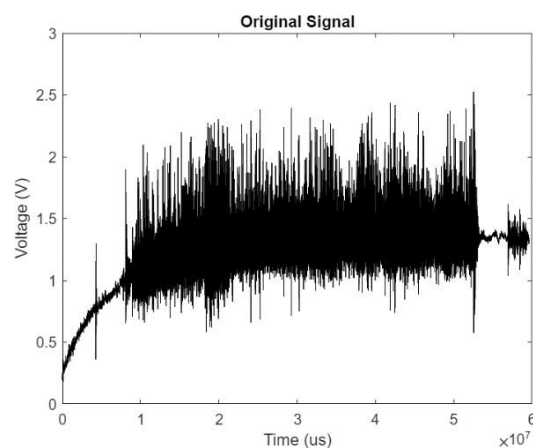


Figure 4.11: Normal Condition Data

Data saved in csv files is plotted in MATLAB, as a graph of voltage (V) vs time (μs). The data is segmented into multiple data to investigate the details. It is split into files with total time duration of 2 seconds. Figure 4.11 demonstrates one of the segmented data.

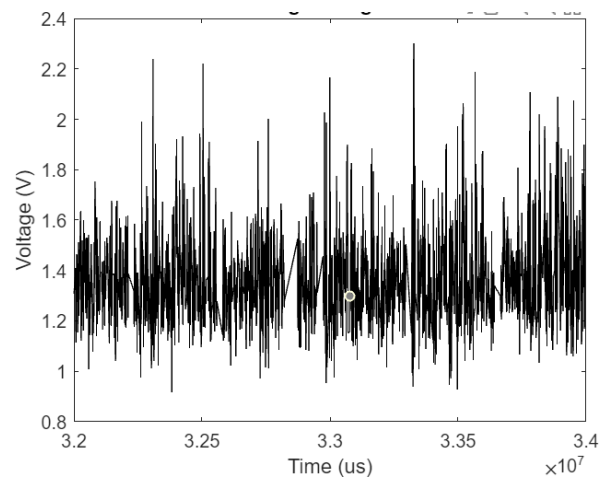


Figure 4.12: Segmented Data

The data are reconstructed and denoised to reduce the noise. Figure 4.13 shows the wavelet transformed data and Figure 4.15 represents the denoised data.

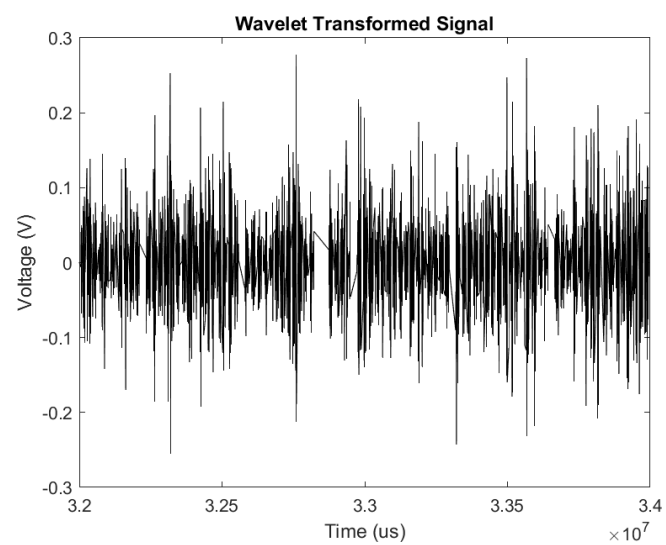


Figure 4.13: Wavelet Transformed Data

The waveform is undergone wavelet transformation in MATLAB for signal compression. Only significant wavelet coefficients are kept and other minor components are discarded. signal is reconstructed from these wavelets. Wavelet reconstruction is done in MATLAB with the built-in application, signal multiresolution analyzer. Figure 4.14 shows the signal multiresolution analyzer application in MATLAB.

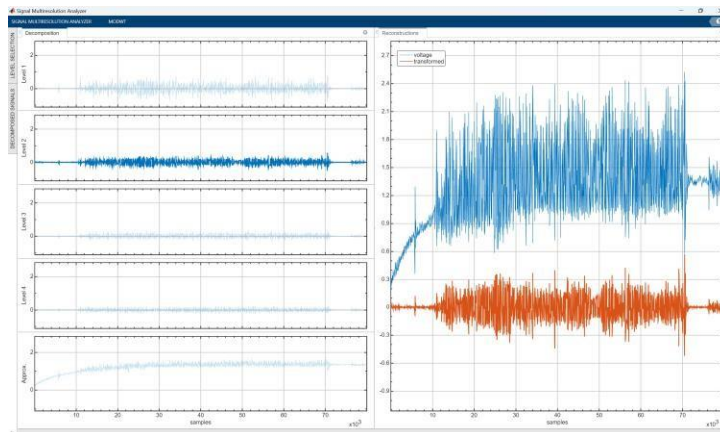


Figure 4.14: Signal Multiresolution Analyzer

From the figure above, blue signal demonstrates the original raw data from the sensor, orange signal is the data after wavelet transformation. Different level selection combinations are tested, however selecting only level 2 can better demonstrate the peaks, hence only level 2 is selected.

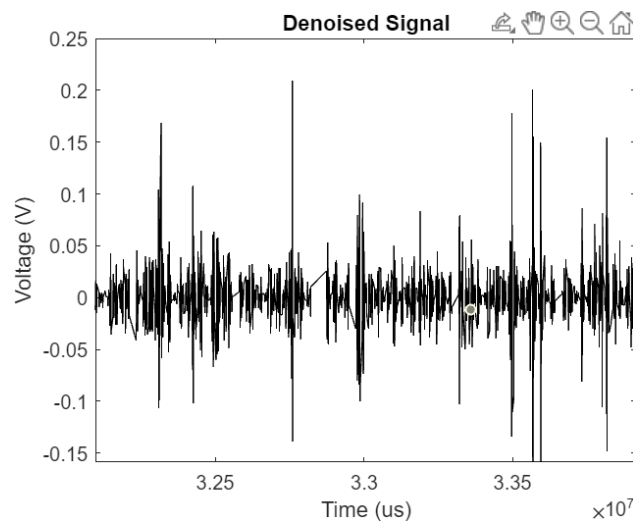


Figure 4.15: Denoised Data

The wavelet transformed data is denoised to improve the signal to noise ratio. In Figure 4.15, the peaks are more obvious compared to those in Figure 4.12. Lastly, FFT of the denoised data is conducted to analyze frequency domain properties of the data. Figure 4.16 shows the FFT of denoised data.

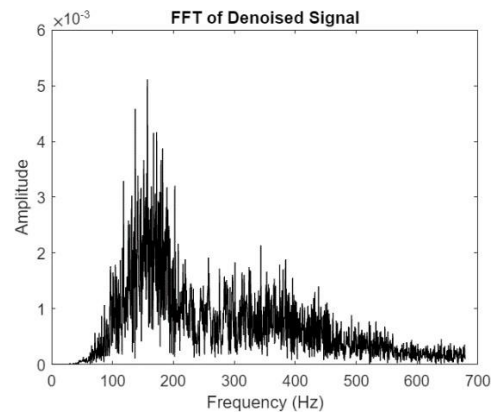


Figure 4.16: FFT of Denoised Data

These plotted data are saved in csv for later work. Figure 4.17 shows the flow chart in MATLAB program for signal processing.

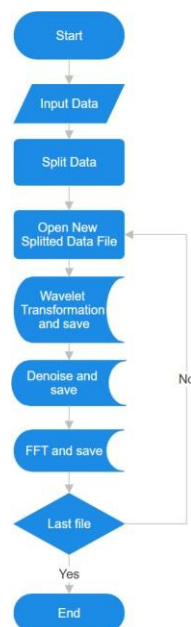


Figure 4.17: Flow Diagram of Signal Processing

4.5 Results

The signal processing steps are repeated for all different data, including normal data, weighted and obstacles conditions.

4.5.1 Normal Conditions

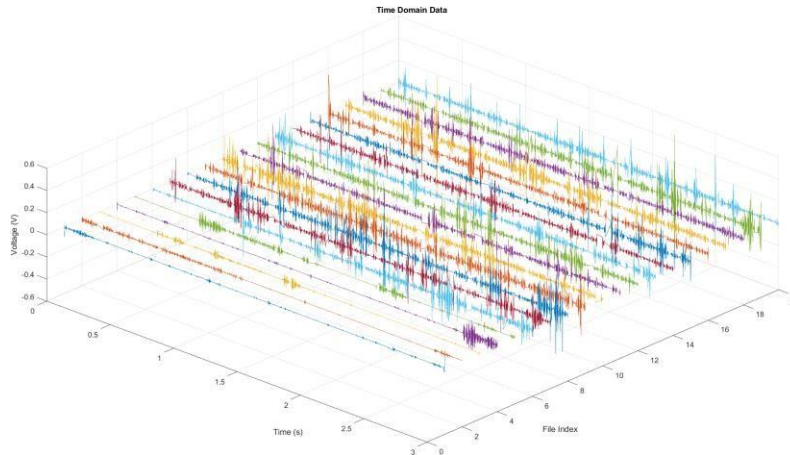


Figure 4.18: Time Domain Data

From the time domain plot, we observed that there are multiple peaks, these peaks are due to vibration on the train. Furthermore, continuous peaks with small time interval (less than 1 second) are highly probably due to gaps in the railway. When train passed the gaps, the front wheels will first meet the perturbation, then the back wheels, hence there should be multiple continuous peaks observed.

Small amplitude at the beginning of the data is because the train is not moving yet. Let us focus on one data, 9th segmented data is shown in figure below.

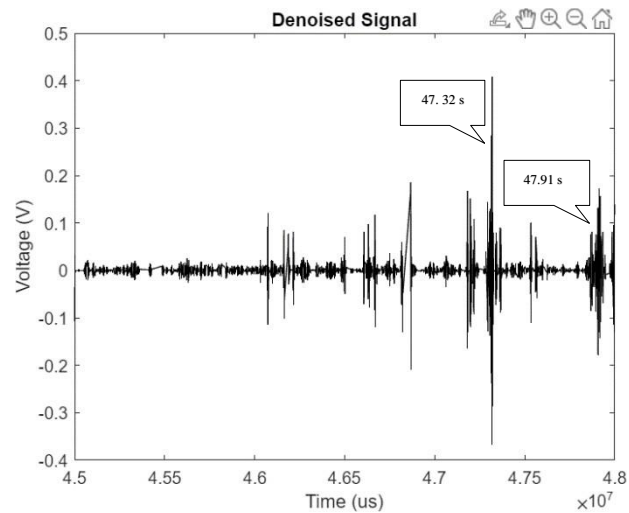


Figure 4.19: 9th Segmented Data from Normal Condition Data

Two peaks are labelled with the time. The time interval between peaks is 0.59 second, hence these peaks are highly probably caused by gap on the railway. It can be validated by capturing video when the sensor is operating.

In another perspective, frequency domain is also very important in data analysis. Figure 4.20 demonstrate the FFT of the data.

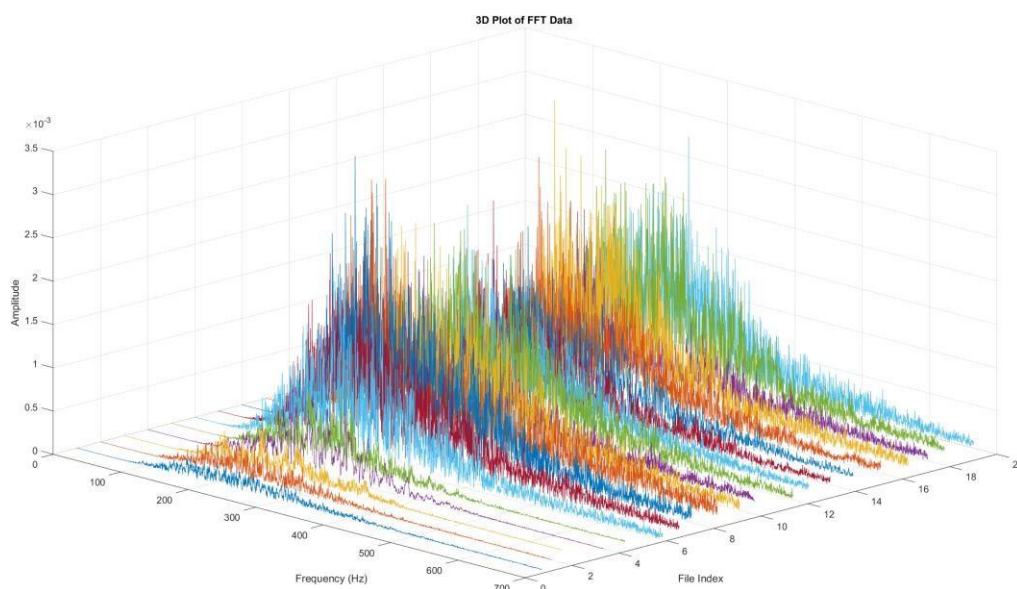


Figure 4.20: FFT of Data

Similar to the time domain plot in Figure 4.18, FFT of the data is plotted in a 3d plot to gather all the data in a plot. From this plot, amplitude and

frequency are the important properties. The plot shows how frequency change in changing time. By comparing the peaks with neighboring plots, we can observe that in that time interval there are something causing abnormal frequency. More data are needed for accurate prediction and monitoring.

4.5.2 Weighted Condition

Figure 4.21 and Figure 4.22 represent the time domain data and frequency domain data of the weighted conditions respectively.

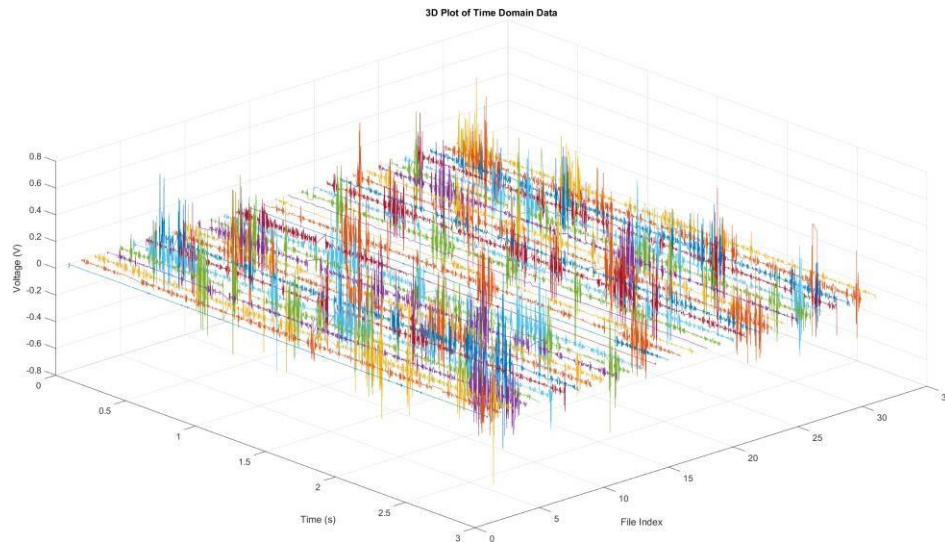


Figure 4.21: Time Domain Data of Weighted Condition

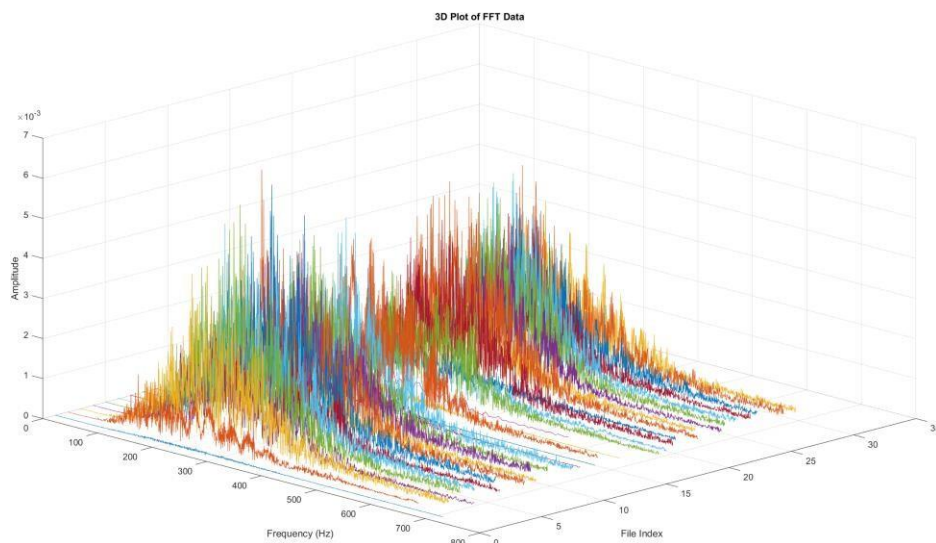


Figure 4.22: Frequency Domain Data of Weighted Condition

In weighted conditions, 6 kg weight is added on top of the train. Figure 4.21 clearly shows that the peaks are more significant as compared to normal conditions in Figure 4.18. Furthermore, in the FFT plot, the maximum amplitude of the peaks is 5×10^{-3} arbitrary units which is higher than those in Figure 4.18 normal condition, having 3×10^{-3} arbitrary units.

4.5.3 Obstacles conditions

Figure 4.23 and Figure 4.24 represent the time domain data and frequency domain data of the obstacles conditions respectively.

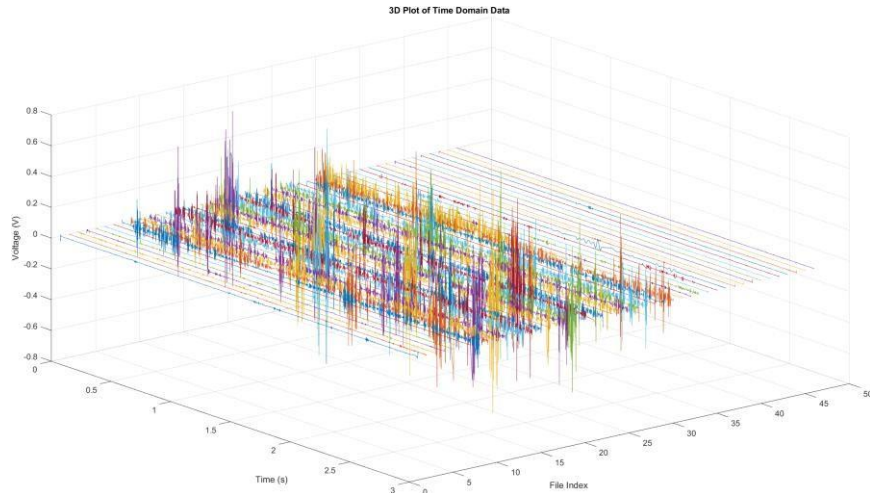


Figure 4.23: Time Domain Data of Obstacles Condition

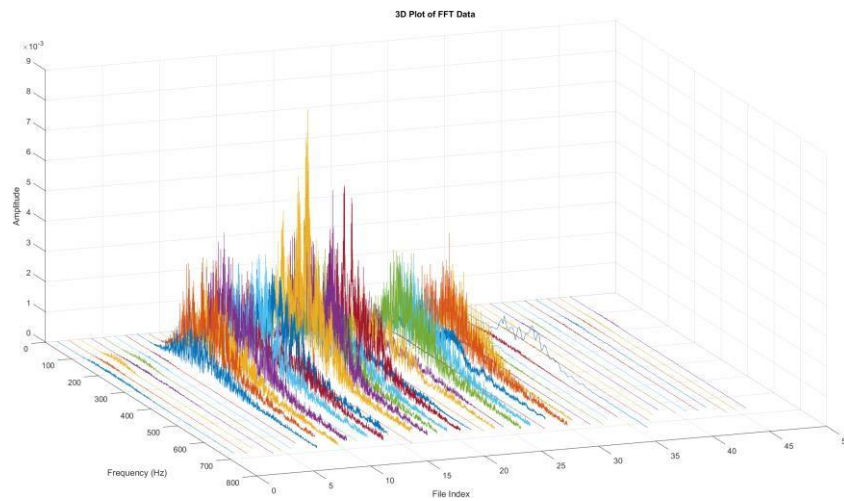


Figure 4.24: Frequency Domain Data of Obstacles Condition

In obstacles conditions, few small rocks are placed on the railway, when the train passed by the rock, it will offtrack and cause abnormal vibrations, these vibrations are treated as the anomalies. Focus on the time domain data shown in Figure 4.23, the peaks are bigger than those in normal conditions, these peaks might be the product of the offtrack event. Apart from that, in Figure 4.24, there is a powerful peak in the FFT which conclude an 8×10^{-3} arbitrary units.

This is also another good evidence that prove that there are anomalies in this set of data.

Different from the weighted conditions, there should be less huge peaks in the time domain as it can only produce when the train is offtrack. In FFT, the average FFT trend is lower than those in weighted conditions, however there will be some abnormal huge peaks that induced by the rock.

4.6 Summary

The fiber laser sensor system is able to capture the vibration of different conditions and feasible to detect the anomalies and different conditions of the railway. By comparing the abnormal data to the normal condition, interesting observation can be observed. The sensor is even possible to detect the speed of the train and change in speed of the train, turning of train and overweight.

In a nutshell, the sensor is very sensitive as it is working in the chaos condition of the laser, any little change in the environment could be capture. In this project, we successfully determine the weighted conditions and obstacles conditions of the mock railway system.

Signal processing using MATLAB is convenient and reliable, it reduced the noise and make it easy for further analysis. Feature extraction and machine learning can be included in future work to improve the accuracy in detecting the anomalies and prediction on the railway conditions.

CHAPTER 5

CONCLUSION AND RECOMMENDATIONS

5.1 Conclusion

In this project, a prototype is designed, it included a laser system of EDFL, data collecting module and sensing arm. The laser system is designed and built in the early part of the project, many testing are done to ensure the laser is operating. The sensors are also finalized after multiple designs for improved sensitivity and reduced noise. The final design of the sensor is a 12 m SMF spooled on plastic cover to increase surface area. Besides that, data collecting module and signal processing is done in Thonny software and MATLAB respectively.

In previous chapter, the results proved that EDFL sensor is able to sense the vibration of the railway system. By applying signal processing techniques, monitoring and prediction on the conditions is possible and reliable. However, large amount data is needed to improve the completeness of the data.

In conclusion fiber laser sensor specifically, Erbium Doped Fiber Laser (EDFL) acoustic vibration sensor is very sensitive and is feasible to be applied in railway health monitoring system. This sensing technique is gaining attention across various industry due to its immunity to electromagnetic interference, ability to cover long distances without signal degradation, light weight and safe to operate.

5.2 Improvements

There are several improvements that can be introduced in this part of the project. Firstly, the improvement in the laser and sensor, the laser source in the prototype is a low power laser with 20 mW operating output power, a slightly higher power laser should improve the performance and the convenience of the laser system. This is because low power laser might not able to capable with the WDM and coupler and can cause low output power to the photodiode.

Secondly, data collecting module can be improve by changing the Raspberry Pi Pico to a WIFI module and log the data to cloud drive. By doing

this, the sensor system can be automated and collected data are even safe and secure.

Thirdly, multiple sensors should be built and attached on the train. This can allow the user to cross compare the results and more observations can be made. Because of the unexpected malfunction of the laser system in midterm of the trimester, there are insufficient time to build more sensors.

Lastly, more different conditions or events of the train need to be collected such as derailment, cracks on rails or wheels, accelerations and decelerations. With large amount and different variety of data, machine learning algorithms can be applied and use to predict the conditions of the train and the railway system.

5.3 Recommendations for Future Work

This project demonstrated the feasibility of the fiber laser sensors by applying laser dynamics properties in monitoring railway health. All collected data is from the mock railway system. There remain several avenues for future work to improve the capabilities of the monitoring system.

Firstly, the sensor can be built as an array and attached to different part for monitoring. Increasing number of sensors also increase the parameters captured and can be applied in signal processing and machine learning.

Secondly, machine learning algorithms such as classifications and clustering can be applied for feature extraction and anomalies detection. Accuracy of the machine learning can be improved by increasing the number of data provided.

REFERENCES

Agensi Pengangkutan Awam Darat (APAD)., 2024. *Perkhidmatan Kereta Api*. [online] Available at <<https://www.apad.gov.my/en/services/railway>> [Accessed 12 February 2024].

Causado-Buelvas, J.D., Gomez-Cardona, N.D. and Torres, P., 2011. Practical Method for engineering Erbium-doped fiber lasers from step-like pulse excitations. *Journal of physics. Conference series*, 274, [e-journal] pp.012017–012017. <https://doi.org/10.1088/1742-6596/274/1/012017>.

Chin, E. S. M., 2021. Transport minister: 166 wounded including 47 seriously hurt in LRT train crash near KLCC. [online] Malay Mail. Available at <<https://www.malaymail.com/news/malaysia/2021/05/24/bernama-at-least-166-hurt-in-lrt-crash-near-klcc/1976729>> [Accessed 12 February 2024].

Dandridge, A., 2011. Fiber Optic Sensors Based on the Mach–Zehnder and Michelson Interferometers. In: *Fiber Optic Sensors* (eds E. Udd and W.B. Spillman). [online] Available at <https://doi.org/10.1002/9781118014103.ch10>

Du, C., Dutta, S., Kurup, P., Yu, T. and Wang, X., 2020. A review of railway infrastructure monitoring using fiber optic sensors. *Sensors and Actuators A: Physical*, [e-journal] 303, p.111728. <https://doi.org/10.1016/j.sna.2019.111728>.

Ge, H., Chua Kim Huat, D., Koh, C.G., Dai, G. and Yu, Y., 2021. Guided wave–based rail flaw detection technologies: state-of-the-art review. *Structural Health Monitoring*, [e-journal] 21(3), pp.1287–1308. <https://doi.org/10.1177/14759217211013110>.

Gong, W., Akbar, M.F., Jawad, G.N., Mohamed, M.F.P. and Wahab, M.N.A. 2022. Nondestructive Testing Technologies for Rail Inspection: A Review. *Coatings*, [e-journal] 12(11), p.1790. <https://doi.org/10.3390/coatings12111790>.

Hecht, J., 2019. *Understanding lasers: an entry-level guide*. Hoboken, New Jersey, Ieee Press. pp.62–66.

James, M., 2023. *Exploring the Top 5 Countries with the Longest Railway Networks - The Trip Discovery*. [online] Available at: <<https://thetripdiscovery.com/exploring-the-top-5-countries-with-the-longest-railway-networks/>> [Accessed 12 February 2024].

Kasap, S. O., 2013. *Optoelectronics and Photonics - Principles and Practices: International Edition*. 2nd ed. U.S.: Pearson Education International.

Kowarik, S., Hussels, M.-T., Chruscicki, S., Münzenberger, S., Lämmerhirt, A., Pohl, P. and Schubert, M., 2020. Fiber Optic Train Monitoring with Distributed Acoustic Sensing: Conventional and Neural Network Data Analysis. *Sensors*, [e-journal] 20(2), p.450. <https://doi.org/10.3390/s20020450>.

M. L. Filograno et al., 2011. *Real-Time Monitoring of Railway Traffic Using Fiber Bragg Grating Sensors*, In: *IEEE Sensors Journal*, vol. 12, no. 1, pp. 85-92, Jan. 2012, doi: 10.1109/JSEN.2011.2135848.

Mathur, P. and Raman, S., 2020. Electromagnetic Interference (EMI): Measurement and Reduction Techniques. *Journal of Electronic Materials*, [e-journal] 49(5), pp.2975–2998. <https://doi.org/10.1007/s11664-020-07979-1>.

Ministry of Transport Malaysia, 2024. *Statistic of Rail Transport, Number of Passengers for Rail Transport Services, 2023*. [pdf] Malaysia: Minister of Transport Malaysia. Available at < [JADUAL 2.7 BILANGAN PENUMPANG BAGI PERKHIDMATAN PENGANGKUTAN REL, SUKU KEEMPAT, 2023.pdf \(mot.gov.my\)](https://www.mot.gov.my/jadual-2-7-bilangan-penumpang-bagi-perkhidmatan-pengangkutan-rel-suku-keempat-2023.pdf)> [Accessed 12 February 2024].

Pisarchik, A.N., Kir'yanov, A.V., Barmenkov, Y.O. and Rider Jaimes-Reátegui, 2005. Dynamics of an erbium-doped fiber laser with pump modulation: theory and experiment. *Journal of the Optical Society of America. B, Optical physics/Journal of the Optical Society of America. B*, [online], 22(10), pp.2107–2107. <https://doi.org/10.1364/josab.22.002107>.

Pua, C.H., Ahmand, H., Harun, S. and De La Rue, R., 2012. Direct airborne acoustic wave modulation of Fabry–Perot fiber laser (FPFL) over 100 kHz of operating bandwidth. *Applied optics*, 51, (15) pp.2772-2777

Pua, C.H., Chong, W.Y. and Ahmad, H., 2013. Instantaneous Response of Wide Area Intrusion Sensor With Long Haul Monitoring Capability. *IEEE Photonics Technology Letters*, [e-journal] 25(23), pp.2255–2258. <https://doi.org/10.1109/lpt.2013.2284608>.

Pua, C.H., Norizan, S.F., Harun, S.W. and Ahmad, H. (2011). Non-membrane optical microphone based on longitudinal modes competition. *Sensors and Actuators A: Physical*, [e-journal] 168(2), pp.281–285. <https://doi.org/10.1016/j.sna.2011.04.034>.

R. Paschotta, 2007. Laser Dynamics - an encyclopedia article. *RP Photonics Encyclopedia*. <https://doi.org/10.61835/za4>. [online] Available at <https://www.rp-photonics.com/laser_dynamics.html>

Rashid, H. and L. Yesmin, 2001. Optical Fiber-Past, Present and Future: A Review. *Khulna University studies*, [e-journal] pp.399–403. <https://doi.org/10.53808/kus.2001.3.1.0112-se>.

S. L. Woon, C. H. Pua, H. S. Lin and F. A. Rahman, 2018. Application of Erbium-Doped Fiber Laser Dynamics in Pipeline Leak Detection and Location Estimation, *2018 IEEE 7th International Conference on Photonics (ICP)*, Langkawi, Malaysia, 2018, [e-journal] pp. 1-3, doi:10.1109/ICP.2018.8533164.

Shahrir, A.H. and Manan, M. M., 2021. *Malaysia's Railway Safety: A Critical Review*. In: MIROS (Malaysian Institute of Road Safety Research), CARS 2021 3rd Conference of Asean Road Safety: Technology and Innovation in Road Safety, Malaysia, 6-7 July 2021. Malaysia: University Kebangsaan Malaysia

Singh, A.K., Swarup, A., Agarwal, A. and Singh, D., 2017. Vision based rail track extraction and monitoring through drone imagery. *ICT Express*. [e-journal] <https://doi.org/10.1016/j.ict.2017.11.010>.

Singh, C., 2023. Machine Learning in Pattern Recognition. *European Journal of Engineering and Technology Research*, [e-journal] 8(2), pp.63–68. <https://doi.org/10.24018/ejeng.2023.8.2.3025>.

T. Erneux and P. Glorieux, 2010. *Laser Dynamics*. Cambridge, U.K.: Cambridge Univ. Press, 2010.

Zhu, W., Qian, L., Helmy, A. S., 2007. Implementation of three functional devices using erbium-doped fibers: an advanced photonics lab. *International Conference on Education and Training in Optics and Photonics, ETOP*.

APPENDICES

Appendix A: Pigtailed Laser Diode Specification Sheet

Technology to lead the Shengshi
Version Mar.2016



980nm Pigtailed Components

Features

- Wavelength : 980nm(Typ.)
- Output power : 20mW
- Threshold current : $I_{th}=10\text{mA}$ (Typ.)
- Operating voltage : $V_{op}=1.5\text{V}$ (Typ.)
- Package : Coaxial Pigtail $\phi 6.0\text{mm}$



Applications

Laser source

Absolute Maximum Ratings

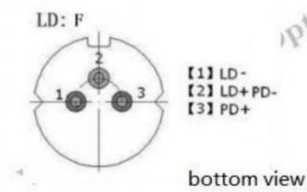
Parameter	Symbol	Min.	Max.	Unit
Fiber Output Power	$P_o(\text{CW})$	-	40	mW
Forward Current(LD)	$I_f(\text{LD})$	-	120	mA
Reverse Voltage(LD)	$V_r(\text{LD})$	-	2	V
Forward Current(PD)	$I_f(\text{PD})$	-	2	mA
Reverse Voltage(PD)	$V_r(\text{PD})$	-	15	V
Storage Temperature	T_{stg}	-40	85	$^{\circ}\text{C}$
Operating Temperature	T_o	-10	50	$^{\circ}\text{C}$
Lead Solder Temperature	-	-	260	$^{\circ}\text{C}$
Lead Solder Time	-	-	10	S

Optical & Electrical Characteristics

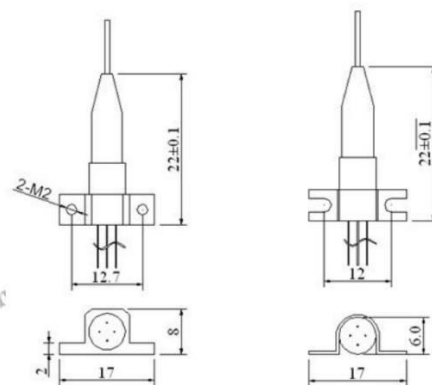
Parameter	Symbol	Min.	Typical	Max.	Unit
Output Power	P_o	-	20	-	mW
Threshold Current	I_{th}	-	10	25	mA
Operating Current	I_f	-	75	85	mA
Operating Voltage	V_f	-	1.5	1.9	V
Monitor Current	I_m	100	-	500	μA
Cent Wavelength	λ_c	975	-	990	nm
Spectral Width(RMS)	$\Delta\lambda$	-	2	3	nm
Spectral Shift	$\Delta\lambda/\Delta T$	-	-	0.2	$\text{nm}/^{\circ}\text{C}$
Fiber	SM(4 μm or 9 μm), MM, other				

Address: 5-floor,Block B Creative Building, Wenzhi St.,Hongshan District,Wuhan, City,Hubei,P.R.China 430074
Contact : Vicky Wang E-mail: vicky@ss-op.com Skype: VICKY_WGY
Cell: 0086-158 7177 5837 Tel: 0086-27-87179709*601

Pin Assignment



Drawing



Order Information


S980-XXXXX

S	980	-X	X	F	X	X
Mode	Wavelength	Connector	Fiber Type	Pin Type	Pigtail Length	Power Range
	980: 980nm	1: FC/APC 2: FC/PC 3: SC/APC 4: SC/PC 5: ST/PC	S4:SM 4um S9:SM 9um M5:MM 50 M6:MM 62.5	F	05: 0.5M 10: 1.0M	P1: >1mW P20: >20mW

Additional requirements can be settled through friendly negotiation.


Shengshi Optical Tech. Co.,Ltd reserves the right to make changes to the product or information contained herein without notice.

Appendix A: Photodiode FGA01FC specification sheet



**InGaAs High Speed Photodiode
with FC/PC Bulkhead**

FGA01FC



Description

The Thorlabs FGA01FC photodiode is ideal for measuring both pulsed and CW fiber light sources, by converting the optical power to an electrical current. The detector is housed in a TO-46 (mod) package with an anode, cathode, and case connection and mounted in an FC bulkhead connector. The photodiode anode produces a current, which is a function of the incident light power and the wavelength. The responsivity $\mathfrak{R}(\lambda)$, can be read from Figure 1 to estimate the amount of photocurrent to expect. This can be converted to a voltage by placing a load resistor (R_L) from the photodiode anode to the circuit ground. The output voltage is derived as:

$$V_o = P \times \mathfrak{R} \times R_L$$


The bandwidth, f_{BW} , and the rise time response, t_R , are determined from the diode capacitance, C_j , and the load resistance, R_L , as shown below. The diode capacitance can be lowered by placing a bias voltage from the photodiode cathode to the circuit ground.


$$f_{BW} = \frac{1}{(2\pi)R_L C_j}, t_R = \frac{0.35}{f_{BW}}$$

Specifications

Specification		Value
Wavelength Range	λ	800 - 1700 nm
Peak Wavelength	λ_p	1550 nm
Responsivity	$\mathfrak{R}(\lambda)$	1.003 A/W
Active Area Diameter	\varnothing	0.12 mm
Rise/Fall Time ($R_L=50 \Omega$, 5 V)	t_r/t_f	0.30 ns
NEP, Typical (1550 nm)	W//Hz	4.50×10^{-15}
Dark Current (5 V)	I_d	0.05 nA (Typ.) 2.00 nA (Max)
Capacitance (5 V)	C_j	2.0 pF (Typ.)
Optical Power Damage Threshold		18 mW
Package		TO-46 (FC/PC)
Sensor Material		InGaAs

Maximum Rating	
Bias Voltage (Reverse)	20 V
Reverse Current	2 mA
ESD	500 V
Operating Temperature	-40 to +75 °C
Storage Temperature	-55 to +125 °C

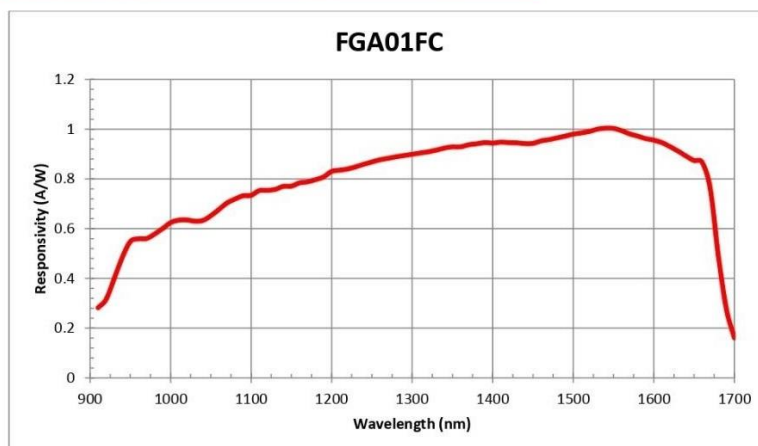




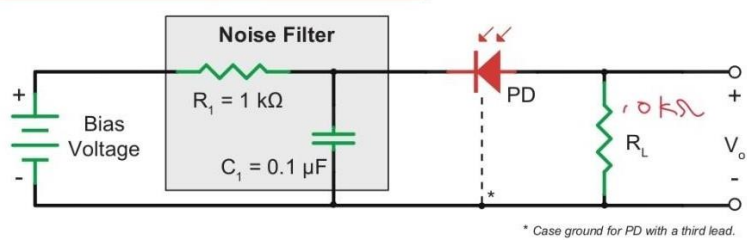
Specifications Subject
to Change without Notice

February 10, 2017
24112-501, Rev F

Typical Spectral Intensity Distribution

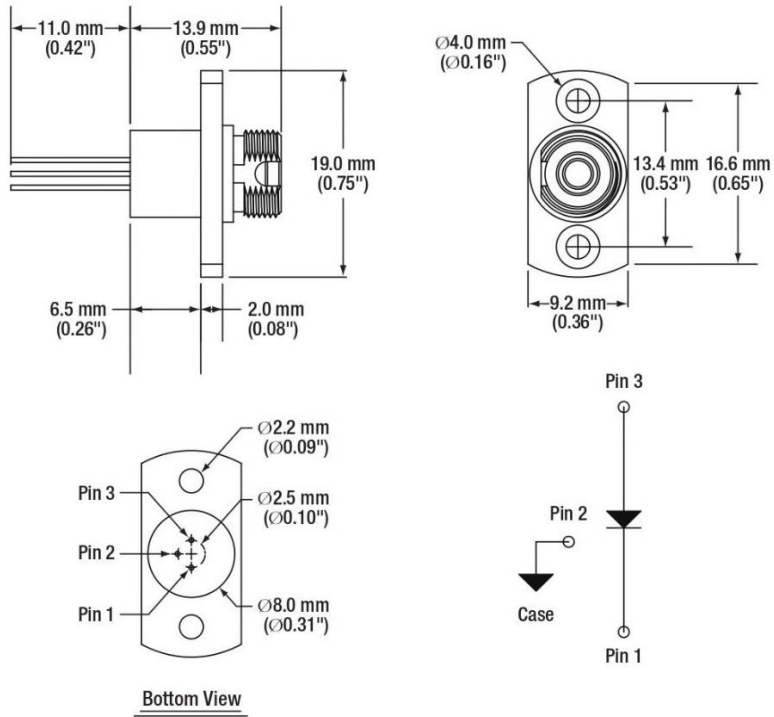


Recommended Circuit



THORLABS

Drawing



Specifications Subject
to Change without Notice

February 10, 2017
24112-S01, Rev F

Precautions and Warranty Information

These products are ESD (electro static discharge) sensitive and as a result are not covered under warranty. In order to ensure the proper functioning of a photodiode care must be given to maintain the highest standards of compliance to the maximum electrical specifications when handling such devices. The photodiodes are particularly sensitive to any value that exceeds the absolute maximum ratings of the product. Any applied voltage in excess of the maximum specification will cause damage and possible complete failure to the product. The user must use handling procedures that prevent any electro static discharges or other voltage surges when handling or using these devices.

Thorlabs, Inc. Life Support and Military Use Application Policy is stated below:

THORLABS' PRODUCTS ARE NOT AUTHORIZED FOR USE AS CRITICAL COMPONENTS IN LIFE SUPPORT DEVICES OR SYSTEMS OR IN ANY MILITARY APPLICATION WITHOUT THE EXPRESS WRITTEN APPROVAL OF THE PRESIDENT OF THORLABS, INC. As used herein:

- 1. Life support devices or systems are devices or systems which, (a) are intended for surgical implant into the body, or (b) support or sustain life, and whose failure to perform, when properly used in accordance with instructions for use provided in the labeling, can be reasonably expected to result in a significant injury to the user.*
- 2. A critical component is any component in a life support device or system whose failure to perform can be reasonably expected to cause the failure of the life support device or system or to affect its safety or effectiveness.*
- 3. The Thorlabs products described in this document are not intended nor warranted for usage in Military Applications.*